Short title: Stress-dependent amplification under horizontal loading

Effects of confining-pressure dependent Lame moduli on the frequency-dependent amplification of a poro-viscoelastic soil layer under horizontal cyclic loading

Kyohei Ueda[1]*

[1]*Disaster Prevention Research Institute, Kyoto University, Gokasho, Uji, Kyoto, 611-0011 Japan*

*Correspondence to:
Kyohei Ueda
Disaster Prevention Research Institute, Kyoto University, Gokasho, Uji, Kyoto, 611-0011 Japan
E-mail address: ueda.kyohei.2v@kyoto-u.ac.jp
TEL: 81-774-38-4092
FAX: 81-774-38-4094

SUMMARY

In this paper, a series of Biot theory-based analytical solutions are proposed to study the dynamic response of a viscoelastic two-phase porous medium subjected to horizontal cyclic loading. To investigate the effect of material dynamic properties' depth (or confining-pressure) dependency, two types of soil stiffness profiles are adopted, along with the constant Lame elastic and loss moduli with depth: the moduli that are linearly increasing with depth and the moduli that are nonlinearly increasing with depth. The influence of the loading frequency, retardation time (or viscous damping), and a newly introduced model parameter that expresses the effect of soil cohesion on the moduli are numerically examined. When the retardation time is small and the dynamic response is periodic, it is demonstrated that the ground surface displacement versus loading frequency is greatly affected by the Lame moduli's depth-dependency; the peak-to-peak period becomes shorter and the amplitude decay tends to be minimal, considering the depth-dependency, particularly in the linearly increasing condition with depth. In addition, the cohesion-related parameter affects not only the periodic displacement amplitude but also the phase characteristics. Furthermore, the effect of the Lame moduli's depth-dependency is investigated on the amplification factor distribution with depth under horizontal loading.

Keywords: poro-viscoelasticity, Lame elastic and loss moduli, confining-pressure dependency, dynamic amplification, horizontal cyclic loading

1. INTRODUCTION

In the engineering design and construction of geotechnical structures, it is essential to accurately evaluate soil behavior subjected to various dynamic or cyclic loads (e.g., seismic loads, wave loads, and traffic loads[1-7]). Dynamic behavior differs from static behavior under dead loads in that the effects of inertia and viscous terms on the equations of motion cannot be ignored; thus, some issues are peculiar to dynamic behavior, such as appropriate modeling of viscous effects and the influence of loading frequency.

Strictly speaking, soils are regarded as a three-phase system consisting of solid particles, voids containing pore water, and empty voids filled with air. However, there is little air deep in the ground, and thus the soil can be described as a fully saturated two-phase porous medium composed of solid skeleton and pore water. In addition, if the influence of pore air (or suction) is not significant, even near the ground surface, the assumption of a two-phase medium can be applied by considering the void as homogeneous pore fluid (or a mixture of water and embedded air).

The formulation of a two-phase porous medium's dynamic behavior originated in the pioneering work of Biot[8-11]. Based on Biot theory, many researchers[12-14] have presented analytical solutions to one-dimensional problems of a saturated poroelastic soil column. Recently, Chen et al.[4, 6] presented a series of analytical solutions for the dynamic response of a nearly saturated seabed subjected to vertical seismic loading. However, several studies[4, 6, 12-16] on Biot theory only considered viscous coupling[17] because of the interaction between the solid skeleton and pore fluid, assuming that the material behavior of the solid skeleton is purely elastic.

When the cyclic behavior of soils is expected to be within a small strain range,

approximately below the level of 10^{-5}, it makes sense to use an elastic model. However, when cyclic strain is greater than this level but less than the order of 10^{-3}, a constitutive model based on the linear viscoelastic theory should be used to represent the cyclic behavior of soils with a reasonable degree of accuracy[18]; in the model, the stress−strain relationship is assumed linear, but a certain energy dissipation (or damping) and hysteretic nature can be logically considered. Researchers[19-21] applied the linear viscoelastic theory to a Biot model to investigate the viscous damping effect. In particular, a recent study by Chen et al.[22] presented a linear poro-viscoelastic model to analyze the one-dimensional dynamic response of a partially saturated soil layer subjected to horizontal and vertical harmonic loadings.

The above previous studies[19-22] considered the effects of viscoelastic properties (i.e., viscous damping) but did not take into account an essential feature of the soil, confining-pressure dependency; material dynamic properties were assumed to be constant with depth. However, several investigators[23-26] have shown that dynamic properties (e.g., shear modulus) of both sandy and clayey soils are strongly affected by the confining-pressure, even at the same void ratio (or relative density). Although such confining-pressure dependency can be numerically considered for seismic or dynamic wave loading, for example, by finite element method (FEM)[27-29], the influence has not been clarified in the form of analytical solutions that can be used to validate the numerical results.

This study proposes analytical solutions based on Biot theory[8-11] to investigate the dynamic response of a viscoelastic two-phase porous medium, of which material dynamic properties are depth (or confining-pressure) dependent. To differentiate between the condition of the constant Lame elastic and loss moduli with depth[22], two types of soil stiffness profiles are adopted in this study: the moduli are assumed to increase linearly

and nonlinearly with depth. Furthermore, the dynamic response of a viscoelastic soil layer subjected to horizontal cyclic loading is numerically discussed in detail, focusing on the influence of loading frequency, retardation time (or viscous damping), and a newly introduced model parameter that expresses the effect of soil cohesion on the moduli.

2. GOVERNING EQUATIONS

2.1. Equilibrium equations for a two-phase porous medium

Soil mass is generally referred to as a three-phase system consisting of solid particles, voids containing pore water, and empty voids filled with air. However, there is little air deep in the ground, and thus the soil can be described as a fully saturated two-phase porous medium. In addition, a nearly saturated (e.g., $S_r > 95\%$) subsurface layer can be treated as a two-phase medium by regarding the void as homogeneous pore fluid (or a mixture of water and embedded air) and assuming that the pore air pressure is equal to the pore water pressure. This study employs a fully dynamic form of Biot's equations[8-11], developed by Zienkiewicz et al.[15], to describe the dynamic behavior of a two-phase porous medium under horizontal cyclic loading.

In consideration of the inertia forces associated with solid skeleton and pore fluid, the overall equilibrium equation for the porous medium is derived as follows.

$$\sigma'_{ij,j} - \alpha\delta_{ij}p_{,j} + \rho g_i = \rho\ddot{u}_i + \rho_f\ddot{\bar{w}}_i, \tag{1}$$

where σ'_{ij} is the effective stress tensor, p is the pore fluid pressure, g_i is the gravitational acceleration vector, and δ_{ij} is the Kronecker delta. Note that the tension is positive for the pore pressure, whereas the compression is positive for the effective stress.

The parameter $\alpha\left(=1-K_b/K_s\right)$ is introduced to account for the compressibility of solid particles; since the bulk modulus of solid particles K_s is much larger than that of the solid skeleton K_b, solid particles are assumed to be incompressible (i.e., $\alpha=1$). ρ is the total density of the porous medium given by

$$\rho=\left(1-n\right)\rho_s+n\rho_f, \tag{2}$$

where ρ_s and ρ_f are the densities of the solid particle and pore fluid, respectively. The average pore fluid relative displacement $\overline{w}$ in Equation (1) is given by $\overline{w}=n\left(w-u\right)$, where n is the soil porosity, and w and u are the displacements of the pore fluid and solid skeleton, respectively.

The flow in the porous medium is assumed to be governed by Darcy's law. The equilibrium equation for the fluid phase can be described as follows.

$$-p_{,i}+\rho_f g_i=\rho_f\ddot{u}_i+\frac{\rho_f}{n}\ddot{\overline{w}}_i+b\dot{\overline{w}}_i, \tag{3}$$

where b is the parameter to account for the viscous resisting force due to the relative movement of the fluid phase to the solid phase, given by

$$b=\frac{\overline{\eta}}{\overline{k}_f}=\frac{\rho_f g}{k_f}, \tag{4}$$

where $\overline{\eta}$ is the fluid viscosity (= 10^{-3} kg/m/s = 1 cP for water) and $\overline{k}_f$ denotes the permeability in the unit square meter. $\rho_f g/\overline{\eta}$ should be multiplied to convert the unit of the permeability into m/s that is used in soil mechanics.

In the following subsections, a stress–strain relationship is derived for each type (i.e., Types A, B, and C) illustrated in Fig. 1. Then, by substituting the relationship into the equilibrium equations (i.e., Equations (1) and (3)), governing equations are derived to

obtain the dynamic response solutions for a poro-viscoelastic soil column under horizontal cyclic loading considering confining-stress dependency.

2.2. Type A: depth-independent material dynamic properties

Viscoelasticity is the property of materials: these are viscous and elastic characteristics of materials when undergoing deformation. While elastic materials are strained when stretched and immediately return to their original state once the stress is removed, viscous materials resist shear flow and strain linearly with time when stress is applied. Viscoelastic behavior can be expressed in a more specific and practical way by introducing spring–dashpot models. In this type of model, spring and dashpot represent the elastic and damping characteristics, respectively, and they are connected in parallel or series. It is worth noting that the dashpot can express only the energy loss characteristics due to the viscosity.

In this study, the energy loss will be assumed to be frequency-dependent (or viscous type) damping[18]; the deformation of a body depends on frequency under cyclic loading. The (generalized) Kelvin–Voigt model has been most widely used to express these characteristics of linear viscoelastic materials[30, 31]; a dashpot is connected in parallel with a spring to represent the damping characteristics, as illustrated in Fig. 2. The stress–strain relationship in the Kelvin–Voigt model can be expressed as follows:

$$\sigma'_{ij} = \lambda\varepsilon\delta_{ij} + 2\mu\varepsilon_{ij} + \lambda'\frac{\partial\varepsilon}{\partial t}\delta_{ij} + 2\mu'\frac{\partial\varepsilon_{ij}}{\partial t}, \tag{5}$$

where $\varepsilon_{ij}\left(=\left(u_{i,j}+u_{j,i}\right)/2\right)$ is the strain tensor, and $\varepsilon\left(=\varepsilon_{ii}\right)$ is the volumetric strain of a solid skeleton. The Lame elastic modulus (or a spring constant), λ and μ, is a parameter indicative of elastic or instantaneous response, whereas the loss modulus (or a

dashpot constant), λ' and μ', represents the energy dissipating characteristics of a viscoelastic body.

In the case of frequency-dependent (or viscous type) damping, these constants can be related to each other as[18]

$$\frac{\lambda'}{\lambda} = \frac{\mu'}{\mu} = \tau , \tag{6}$$

where τ is called the retardation time in seconds, which denotes the resistance of the viscosity to the elastic deformation of a body. The response becomes perfectly elastic as the retardation time approaches zero. As a way of expressing the damping characteristics, the energy loss ΔW (or the hysteresis loop area) per cycle is used in a normalized way with respect to the maximum stored energy (or the strain energy stored in a perfectly elastic body) W. This is because the energy loss itself is a function of strain amplitude and does not properly express the intrinsic property. The normalized quantity $\Delta W / W$ is related to the loss coefficient η and the damping ratio D, which are frequently used in soil dynamics to indicate damping characteristics[18], as follows.

$$\eta = 2D = \frac{1}{2\pi}\frac{\Delta W}{W} = \frac{\mu'\omega}{\mu} = \tau\omega , \tag{7}$$

where ω is the angular frequency. The frequency-dependent damping in Equation (7) is caused by the use of the viscous dashpot, which correlates the stress with the time rate of strain. Note that some laboratory experiments and field investigations have suggested a frequency-independent (or non-viscous) damping under seismic loading[18]; in this case, it may be difficult to apply the viscous type formulations specified in Equations (5) through (7) directly. However, this paper sheds light on introducing the confining-pressure dependency of material dynamic properties into the viscous type Kelvin–Voigt

model, leaving the non-viscous type Kelvin–Voigt model for future work.

Following Chen et al.[22], the constitutive equation for the compressible pore fluid is formulated by

$$p = -M\left(\overline{w}_{i,i} + \alpha u_{i,i}\right) = -M\left(\overline{w}_{i,i} + \alpha\varepsilon\right), \tag{8}$$

where $-\overline{w}_{i,i}$ denotes the volumetric strain of pore fluid. The parameter M is introduced to account for the compressibility of solid particles and pore fluid and can be expressed as follows.

$$M = \frac{K_s^2}{K_d - K_b}, \quad K_d = K_s\left[1 + n\left(\frac{K_s}{K_f} - 1\right)\right], \tag{9}$$

where K_s, K_b, and K_f are the bulk modulus of solid particles, solid skeleton, and pore fluid, respectively. When the degree of saturation is sufficiently high (e.g., $S_r > 95\%$), the bulk modulus of homogeneous pore fluid (or a mixture of water and embedded air) can be given as[32, 33]

$$\frac{1}{K_f} = \frac{S_r}{K_w} + \frac{1 - S_r}{K_a}, \tag{10}$$

where K_w and K_a are the bulk modulus of water and air, respectively. It is noted that partially saturated soils containing a discontinuous gas phase in the form of bubbles embedded in a liquid phase[34] are considered here.

As described in the following section, the parameters α and M in Equation (8) do not affect the governing equations for horizontal loading (e.g., Equations (21) and (22)) but do affect the governing equations for vertical loading as studied by Chen et al.[22], in which the Lame elastic moduli were assumed to be constant (i.e., depth-independent). This paper focuses only on the horizontal vibration response of soils with depth-

dependent elastic moduli, but the depth-dependency effect on the vertical vibration should be studied in the future.

By substituting the constitutive equations (5) and (8) into the overall equilibrium equation (1) in the absence of body forces, the overall governing equation for the poro-viscoelastic medium, of which material dynamic properties are confining-stress independent, can be derived as follows[22].

$$\mu u_{i,jj} + \left(\mu + \lambda + \alpha^2 M\right) u_{j,ji} + \mu' \dot{u}_{i,jj} + \left(\mu' + \lambda'\right) \dot{u}_{j,ji} + \alpha M \overline{w}_{j,ji} = \rho \ddot{u}_i + \rho_f \ddot{\overline{w}}_i , \quad (11)$$

where the Lame elastic and loss moduli are assumed to be depth-independent. In addition, substituting Equation (8) into the equilibrium equation (3) for the fluid phase derives the governing equation for the fluid phase given by[22]

$$\alpha M u_{j,ji} + M \overline{w}_{j,ji} = \rho_f \ddot{u}_i + \frac{\rho_f}{n} \ddot{\overline{w}}_i + b \dot{\overline{w}}_i . \quad (12)$$

These equations are the governing equations to be solved in a coupled manner considering the appropriate boundary conditions when porous medium's material dynamic properties are confining-stress independent (see Fig. 1(a)).

2.3. Type B: material dynamic properties linearly dependent on depth

When the Lame elastic moduli in Equation (5) are linearly dependent on depth (or confining-stress), as shown in Fig. 1(b), they can be given as a function of depth z as expressed below.

$$\lambda(z) = \frac{z_0 + z}{z_0 + z_{\text{ref}}} \lambda_{\text{ref}} , \quad \mu(z) = \frac{z_0 + z}{z_0 + z_{\text{ref}}} \mu_{\text{ref}} , \quad (13)$$

where λ_{ref} and μ_{ref} correspond to the Lame elastic moduli at depth z_{ref}, and z_0 is a model parameter that provides for non-zero modulus at the ground surface. Although the

depth dependency is generally nonlinear regardless of soil type[35, 36], as described in the next subsection, Type B is also considered in this study for the following reasons: (1) Formulation is easier than for Type C. (2) Some literature reports depth dependency that is close to linear, although limited in number[35]. It is noted that the loss moduli λ' and μ' also take the same functional form as Equation (13) because of Equation (6). Here, let us consider a different way of expressing the depth-dependency in Equation (13) using the effective confining pressure σ'_{m}. Using the internal friction angle ϕ'_{f} and cohesion c of soil, Equation (13) can be rewritten as

$$\lambda(z)=\frac{c\cot\phi'_{\mathrm{f}}+\sigma'_{\mathrm{m}}}{c\cot\phi'_{\mathrm{f}}+\left(\sigma'_{\mathrm{m}}\right)_{\mathrm{ref}}}\lambda_{\mathrm{ref}},\quad \mu(z)=\frac{c\cot\phi'_{\mathrm{f}}+\sigma'_{\mathrm{m}}}{c\cot\phi'_{\mathrm{f}}+\left(\sigma'_{\mathrm{m}}\right)_{\mathrm{ref}}}\mu_{\mathrm{ref}}, \tag{14}$$

where $\left(\sigma'_{\mathrm{m}}\right)_{\mathrm{ref}}$ denotes the effective confining pressure at depth z_{ref}. Comparison of Equation (14) with Equation (13) indicates that the parameter z_0 mainly represents the effect of soil cohesion and can be given by

$$z_0=\frac{3}{1+2K_0}\frac{c\cot\phi'_{\mathrm{f}}}{\gamma'}, \tag{15}$$

where γ' is the effective unit volume weight of soil, and K_0 is the static earth pressure coefficient. It is noted that since the change in K_0 is not significant in the level ground, the parameter z_0 can be estimated once the strength constants (i.e., ϕ'_{f} and c) are obtained in addition to γ'; alternatively, it can be determined based on the shear wave velocity ($V_{\mathrm{s}}=\sqrt{\mu/\rho}$) at the ground surface using the second equation in Equation (13).

Then, to simplify the governing equation formulation, variable z in Equation (13) is transformed into a new variable $\tilde{z}$ as follows.

$$\tilde{z}=z_0+z,\quad \tilde{z}_{\mathrm{ref}}=z_0+z_{\mathrm{ref}}. \tag{16}$$

Accordingly, by substituting Equations (5) and (8) into Equation (1) with the use of Equations (13) and (16), the overall governing equation for the poro-viscoelastic medium of which the Lame elastic and loss moduli are linearly dependent on depth can be derived, instead of Equation (11).

$$\begin{aligned}&\mu u_{i,jj}+\left(\mu+\lambda+\alpha^2 M\right)u_{j,ji}+\mu' \dot{u}_{i,jj}+\left(\mu'+\lambda'\right)\dot{u}_{j,ji}+\alpha M \overline{w}_{j,ji}\\&+\frac{\tilde{z}_{,i}}{\tilde{z}_{\mathrm{ref}}}\lambda_{\mathrm{ref}}u_{j,j}+\frac{\tilde{z}_{,j}}{\tilde{z}_{\mathrm{ref}}}\mu_{\mathrm{ref}}\left(u_{i,j}+u_{j,i}\right)+\frac{\tilde{z}_{,i}}{\tilde{z}_{\mathrm{ref}}}\lambda_{\mathrm{ref}}\tau\dot{u}_{j,j}+\frac{\tilde{z}_{,j}}{\tilde{z}_{\mathrm{ref}}}\mu_{\mathrm{ref}}\tau\left(\dot{u}_{i,j}+\dot{u}_{j,i}\right).\\&=\rho\ddot{u}_i+\rho_f\ddot{\overline{w}}_i\end{aligned}\qquad(17)$$

Note that the governing equation for the fluid phase is the same as Equation (12), but the partial derivation in the vertical direction shall be performed on variable $\tilde{z}$ in Equation (16). When a porous medium's material dynamic properties are linearly dependent on depth (see Fig. 1(b)), Equations (17) and (12) are the governing equations that will be solved in a coupled manner.

2.4. Type C: material dynamic properties nonlinearly dependent on depth

When the Lame elastic moduli in Equation (5) are nonlinearly dependent on depth (or confining-stress), as shown in Fig. 1(c), they can be given as a function of depth z, as expressed below.

$$\lambda(z)=\left(\frac{z_0+z}{z_0+z_{\mathrm{ref}}}\right)^{m_G}\lambda_{\mathrm{ref}},\quad \mu(z)=\left(\frac{z_0+z}{z_0+z_{\mathrm{ref}}}\right)^{m_G}\mu_{\mathrm{ref}},\qquad(18)$$

where λ_{ref} and μ_{ref} denote the Lame elastic moduli at depth z_{ref}, and z_0 and $m_G\left(\neq 1.0\right)$ are model parameters. m_G has been reported to be about 0.50 for many laboratory tested soils, particularly clean sands and pure clays; however, a wide variety of literature suggests that m_G may take values between 0.35 and 0.90[35]. It is also

suggested that m_G could be greater than 1.0 depending on the soil type and age[36]. When the depth distribution of μ or V_s is available, the model parameters in Equation (18) can be easily estimated[37]. It is noted that the loss moduli λ' and μ' also take the same functional form as Equation (18) because of Equation (6). By considering Equation (15), the above equations can be rewritten as

$$\lambda(z)=\left(\frac{c\cot\phi'_{\mathrm{f}}+\sigma'_{\mathrm{m}}}{c\cot\phi'_{\mathrm{f}}+(\sigma'_{\mathrm{m}})_{\mathrm{ref}}}\right)^{m_G}\lambda_{\mathrm{ref}},\quad \mu(z)=\left(\frac{c\cot\phi'_{\mathrm{f}}+\sigma'_{\mathrm{m}}}{c\cot\phi'_{\mathrm{f}}+(\sigma'_{\mathrm{m}})_{\mathrm{ref}}}\right)^{m_G}\mu_{\mathrm{ref}}. \tag{19}$$

As mentioned in the previous subsection, the parameter z_0 in Equation (18) can represent mainly the influence of soil cohesion, and be estimated based on the strength constants (i.e., ϕ'_{f} and c) or V_s at the ground surface.

By substituting Equations (5) and (8) into Equation (1) with the use of Equations (18) and (16), the overall governing equation for the poro-viscoelastic medium of which the Lame elastic and loss moduli are nonlinearly dependent on depth can be derived as follows.

$$\begin{aligned}
&\mu u_{i,jj}+\left(\mu+\lambda+\alpha^2M\right)u_{j,ji}+\mu'\dot{u}_{i,jj}+\left(\mu'+\lambda'\right)\dot{u}_{j,ji}+\alpha M\overline{w}_{j,ji}\\
&+\frac{m_G}{\tilde{z}_{\mathrm{ref}}}\left(\frac{\tilde{z}}{\tilde{z}_{\mathrm{ref}}}\right)^{m_G-1}\lambda_{\mathrm{ref}}u_{j,j}+\frac{m_G}{\tilde{z}_{\mathrm{ref}}}\left(\frac{\tilde{z}}{\tilde{z}_{\mathrm{ref}}}\right)^{m_G-1}\mu_{\mathrm{ref}}\left(u_{i,j}+u_{j,i}\right)\\
&+\frac{m_G}{\tilde{z}_{\mathrm{ref}}}\left(\frac{\tilde{z}}{\tilde{z}_{\mathrm{ref}}}\right)^{m_G-1}\lambda_{\mathrm{ref}}\tau\dot{u}_{j,j}+\frac{m_G}{\tilde{z}_{\mathrm{ref}}}\left(\frac{\tilde{z}}{\tilde{z}_{\mathrm{ref}}}\right)^{m_G-1}\mu_{\mathrm{ref}}\tau\left(\dot{u}_{i,j}+\dot{u}_{j,i}\right)\\
&=\rho\ddot{u}_i+\rho_f\ddot{\overline{w}}_i
\end{aligned}. \tag{20}$$

Note that the governing equation for the fluid phase is the same as Equation (12), but the partial derivation in the vertical direction shall be performed on variable $\tilde{z}$ in Equation (16). When a porous medium's material dynamic properties are nonlinearly dependent on depth (see Fig. 1(c)), Equations (20) and (12) are the governing equations that should

be solved in a coupled manner.

3. ANALYTICAL SOLUTIONS UNDER HORIZONTAL VIBRATION

Fig. 3 explains the geometry and boundary conditions of the physical model subjected to horizontal loading. The ground surface (z = 0) is assumed to be a free drainage boundary, whereas the bottom of the soil column ($z = L$) is assumed to be impermeable. In the case of horizontal cyclic stress loading that is acting on the ground surface (e.g., cyclic traffic loading), as shown in Fig. 3(a), the horizontal displacement response at the ground surface shall be calculated under a fixed bottom condition. When the bottom is subjected to horizontal cyclic displacement loading (e.g., seismic loading), as shown in Fig. 3(b), the ground surface cyclic response will be calculated under a stress-free surface boundary condition.

3.1. Type A: depth-independent material dynamic properties

When the material dynamic properties of the soil column are depth-independent, the governing equations (11) and (12) can be reduced by ignoring the horizontal partial derivative as follows[22].

$$\mu \frac{\partial^2 u_x}{\partial z^2} + \mu' \frac{\partial^3 u_x}{\partial z^2 \partial t} - \rho \frac{\partial^2 u_x}{\partial t^2} - \rho_f \frac{\partial^2 \overline{w}_x}{\partial t^2} = 0 , \tag{21}$$

$$\rho_f \frac{\partial^2 u_x}{\partial t^2} + \frac{\rho_f}{n} \frac{\partial^2 \overline{w}_x}{\partial t^2} + b \frac{\partial \overline{w}_x}{\partial t} = 0 . \tag{22}$$

By substituting Equation (21) and its time derivative into the time derivative of Equation (22), the governing equation for the soil skeleton displacement can be derived as

$$\frac{\partial^3 u_x}{\partial t^3}+a_1\frac{\partial^2 u_x}{\partial t^2}+a_2\frac{\partial^4 u_x}{\partial z^2\partial t^2}+a_3\frac{\partial^3 u_x}{\partial z^2\partial t}+a_4\frac{\partial^2 u_x}{\partial z^2}=0, \tag{23}$$

with

$$a_1=-\frac{\rho nb}{\left(n\rho_f-\rho\right)\rho_f},\quad a_2=\frac{\mu'}{n\rho_f-\rho},\quad a_3=\frac{\mu' nb+\mu\rho_f}{\left(n\rho_f-\rho\right)\rho_f},\quad a_4=\frac{\mu nb}{\left(n\rho_f-\rho\right)\rho_f}. \tag{24}$$

Assuming the following form for the horizontal displacement response under cyclic loading,

$$u_x\left(z,t\right)=\overline{u}_x\exp\left[i\left(\omega t-zk_s\right)\right], \tag{25}$$

where $\overline{u}_x$ is the displacement amplitude, ω is the angular frequency, and k_s is a complex number for shear wave, Equation (23) can be further reduced to

$$\left(a_2\omega^2-a_3i\omega-a_4\right)k_s^2-a_1\omega^2-i\omega^3=0. \tag{26}$$

Solving the above equation with respect to k_s, the displacement of the solid skeleton can be finally given by

$$u_x\left(z,t\right)=\left[c_1\exp\left(-ik_sz\right)+c_2\exp\left(ik_sz\right)\right]\exp\left(i\omega t\right). \tag{27}$$

The coefficients $c_i\left(i=1,2\right)$ can be determined by considering the boundary conditions for the stress loading at the ground surface (Fig. 3(a)),

$$\tau=\tau_0\exp\left(i\omega t\right)\quad\text{at}\quad z=0, \tag{28}$$

$$u_x=0\quad\text{at}\quad z=L, \tag{29}$$

where τ_0 denotes the shear stress amplitude, or the boundary conditions for the displacement loading at the bottom (Fig. 3(b)),

$$\tau=0\quad\text{at}\quad z=0, \tag{30}$$

$$u_x=u_0\exp\left(i\omega t\right)\quad\text{at}\quad z=L, \tag{31}$$

where u_0 is the bottom displacement amplitude.

By solving Equations (21) and (22) for the average relative fluid displacement $\overline{w}_x$ demonstrates that it takes a similar form as the soil skeleton displacement u_x (see Equation (27)), as expressed below.

$$\overline{w}_x\left(z,t\right)=\left[c_1\eta_1\exp\left(-ik_sz\right)+c_2\eta_2\exp\left(ik_sz\right)\right]\exp\left(i\omega t\right), \tag{32}$$

with

$$\eta_1=\eta_2=\frac{k_s^2\left(\mu+i\omega\mu'\right)-\rho\omega^2}{\rho_f\omega^2}. \tag{33}$$

The horizontal displacement $\overline{w}_x$ does not contribute to the pore fluid pressure given by Equation (8) since the displacement direction is orthogonal to variable z (i.e., depth). However, the explicit theoretical form can be used to validate numerical simulations of a two-phase porous medium.

3.2. Type B: material dynamic properties linearly dependent on depth

When the material dynamic properties of the soil column are linearly dependent on depth, the governing equation (17) can be reduced to

$$\begin{aligned}&\frac{\tilde{z}}{\tilde{z}_{\text{ref}}}\mu_{\text{ref}}\frac{\partial^2u_x}{\partial\tilde{z}^2}+\frac{\tilde{z}}{\tilde{z}_{\text{ref}}}\mu'_{\text{ref}}\frac{\partial^3u_x}{\partial\tilde{z}^2\partial t}+\frac{1}{\tilde{z}_{\text{ref}}}\mu_{\text{ref}}\frac{\partial u_x}{\partial\tilde{z}}+\frac{1}{\tilde{z}_{\text{ref}}}\mu'_{\text{ref}}\frac{\partial^2u_x}{\partial\tilde{z}\partial t}\\&-\rho\frac{\partial^2u_x}{\partial t^2}-\rho_f\frac{\partial^2\overline{w}_x}{\partial t^2}=0\end{aligned}, \tag{34}$$

under horizontal loading conditions. It is noted that the governing equation for the fluid phase is the same as Equation (22), regardless of the confining-stress dependency.

By substituting Equation (34) and its time derivative into the time derivative of Equation (22), the governing equation for soil skeleton displacement can be derived as follows.

$$\begin{aligned}&\frac{\partial^3 u_x}{\partial t^3}+a_1\frac{\partial^2 u_x}{\partial t^2}+\frac{\tilde{z}}{\tilde{z}_{\text{ref}}}\frac{\partial^2}{\partial \tilde{z}^2}\left(\tilde{a}_2\frac{\partial^2 u_x}{\partial t^2}+\tilde{a}_3\frac{\partial u_x}{\partial t}+\tilde{a}_4 u_x\right)\\&+\frac{1}{\tilde{z}_{\text{ref}}}\frac{\partial}{\partial \tilde{z}}\left(\tilde{a}_2\frac{\partial^2 u_x}{\partial t^2}+\tilde{a}_3\frac{\partial u_x}{\partial t}+\tilde{a}_4 u_x\right)=0\end{aligned},\tag{35}$$

with

$$\tilde{a}_2=\frac{\mu'_{\text{ref}}}{n\rho_f-\rho},\quad \tilde{a}_3=\frac{\mu'_{\text{ref}}nb+\mu_{\text{ref}}\rho_f}{\left(n\rho_f-\rho\right)\rho_f},\quad \tilde{a}_4=\frac{\mu_{\text{ref}}nb}{\left(n\rho_f-\rho\right)\rho_f}.\tag{36}$$

Assuming the following form for the horizontal displacement response under cyclic loading,

$$u_x\left(\tilde{z},t\right)=\overline{u}_x\exp\left(i\omega t\right)F\left(\tilde{z}\right),\tag{37}$$

where F is an unknown function of $\tilde{z}$ that is to be solved, Equation (35) can be rewritten as

$$\tilde{z}\frac{d^2F}{d\tilde{z}^2}+\frac{dF}{d\tilde{z}}+A\left(\omega\right)F=\frac{d}{d\tilde{z}}\left(\tilde{z}\frac{dF}{d\tilde{z}}\right)+A\left(\omega\right)F=0,\tag{38}$$

with

$$A\left(\omega\right)=\frac{a_1\omega^2+i\omega^3}{\tilde{a}_2\omega^2-\tilde{a}_3 i\omega-\tilde{a}_4}\tilde{z}_{\text{ref}}.\tag{39}$$

According to Courant and Hilbert[38], Equation (38) is classified as a Sturm-Liouville type differential equation and its solution can be given by

$$F\left(\tilde{z}\right)=c_3J_0\left(2\sqrt{A\tilde{z}}\right)+c_4Y_0\left(2\sqrt{A\tilde{z}}\right),\tag{40}$$

where $c_i\left(i=3,4\right)$ are coefficients to be determined depending on boundary conditions, and $J_n\left(\bullet\right)$ and $Y_n\left(\bullet\right)$ are the Bessel functions of the first and second kinds, respectively.

$$J_n(x)=\sum_{m=0}^{\infty}\frac{(-1)^m}{m!\Gamma(m+n+1)}\left(\frac{x}{2}\right)^{2m+n}, \tag{41}$$

$$Y_n(x)=\frac{\cos(n\pi)J_n(x)-J_{-n}(x)}{\sin(n\pi)}. \tag{42}$$

Substituting Equation (40) into Equation (37) produces the displacement solution of the solid skeleton under horizontal cyclic loading as

$$u_x(\tilde{z},t)=\left[c_3J_0\left(2\sqrt{A\tilde{z}}\right)+c_4Y_0\left(2\sqrt{A\tilde{z}}\right)\right]\exp(i\omega t). \tag{43}$$

Then, the shear strain can be calculated by partial differentiation of Equation (43) with $\tilde{z}$ as follows.

$$\frac{\partial u_x(\tilde{z},t)}{\partial\tilde{z}}=-\sqrt{\frac{A}{\tilde{z}}}\left[c_3J_1\left(2\sqrt{A\tilde{z}}\right)+c_4Y_1\left(2\sqrt{A\tilde{z}}\right)\right]\exp(i\omega t). \tag{44}$$

The coefficients $c_i\,(i=3,4)$ in Equations (43) and (44) can be obtained under appropriate boundary conditions: Equations (28) and (29) for the ground surface stress loading (Fig. 3(a)); Equations (30) and (31) for the bottom displacement loading (Fig. 3(b)).

By solving Equations (34) and (22) for the average relative fluid displacement, $\overline{w}_x$ is found to take a similar form as the soil skeleton displacement u_x (see Equation (43)), as expressed below.

$$\overline{w}_x(\tilde{z},t)=\left[c_3\eta_3J_0\left(2\sqrt{A\tilde{z}}\right)+c_4\eta_4Y_0\left(2\sqrt{A\tilde{z}}\right)\right]\exp(i\omega t). \tag{45}$$

The coefficients $\eta_i\,(i=3,4)$ can be derived by substituting Equations (43) and (45) into Equation (34) as

$$\eta_1 = \frac{A\left(\mu_{\text{ref}} + i\omega\mu'_{\text{ref}}\right)}{2\rho_f\omega^2\tilde{z}_{\text{ref}}}\left[1 + \frac{J_1\left(2\sqrt{A\tilde{z}}\right)}{\sqrt{A\tilde{z}}J_0\left(2\sqrt{A\tilde{z}}\right)} - \frac{J_2\left(2\sqrt{A\tilde{z}}\right)}{J_0\left(2\sqrt{A\tilde{z}}\right)}\right] - \frac{\rho}{\rho_f}. \tag{46}$$

$$\eta_2 = \frac{A\left(\mu_{\text{ref}} + i\omega\mu'_{\text{ref}}\right)}{2\rho_f\omega^2\tilde{z}_{\text{ref}}}\left[1 + \frac{Y_1\left(2\sqrt{A\tilde{z}}\right)}{\sqrt{A\tilde{z}}Y_0\left(2\sqrt{A\tilde{z}}\right)} - \frac{Y_2\left(2\sqrt{A\tilde{z}}\right)}{Y_0\left(2\sqrt{A\tilde{z}}\right)}\right] - \frac{\rho}{\rho_f}. \tag{47}$$

3.3. Type C: material dynamic properties nonlinearly dependent on depth

When the material dynamic properties of the soil column are nonlinearly dependent on depth, the governing equation (20) can be reduced to

$$\begin{aligned}&\left(\frac{\tilde{z}}{\tilde{z}_{\text{ref}}}\right)^{m_G}\mu_{\text{ref}}\frac{\partial^2 u_x}{\partial\tilde{z}^2} + \left(\frac{\tilde{z}}{\tilde{z}_{\text{ref}}}\right)^{m_G}\mu'_{\text{ref}}\frac{\partial^3 u_x}{\partial\tilde{z}^2\partial t} + \frac{m_G}{\tilde{z}_{\text{ref}}}\left(\frac{\tilde{z}}{\tilde{z}_{\text{ref}}}\right)^{m_G-1}\mu_{\text{ref}}\frac{\partial u_x}{\partial\tilde{z}}\\ &+\frac{m_G}{\tilde{z}_{\text{ref}}}\left(\frac{\tilde{z}}{\tilde{z}_{\text{ref}}}\right)^{m_G-1}\mu'_{\text{ref}}\frac{\partial^2 u_x}{\partial\tilde{z}\partial t} - \rho\frac{\partial^2 u_x}{\partial t^2} - \rho_f\frac{\partial^2\overline{w}_x}{\partial t^2} = 0\end{aligned}, \tag{48}$$

under horizontal loading conditions. It is worth noting that the governing equation for the fluid phase is the same as Equation (22), regardless of the confining-stress dependency. By substituting Equation (48) and its time derivative into the time derivative of Equation (22), the governing equation for the soil skeleton displacement can be derived as follows.

$$\begin{aligned}&\frac{\partial^3 u_x}{\partial t^3} + a_1\frac{\partial^2 u_x}{\partial t^2} + \left(\frac{\tilde{z}}{\tilde{z}_{\text{ref}}}\right)^{m_G}\frac{\partial^2}{\partial\tilde{z}^2}\left(a_8\frac{\partial^2 u_x}{\partial t^2} + a_9\frac{\partial u_x}{\partial t} + a_{10}u_x\right)\\ &+\frac{m_G}{\tilde{z}_{\text{ref}}}\left(\frac{\tilde{z}}{\tilde{z}_{\text{ref}}}\right)^{m_G-1}\frac{\partial}{\partial\tilde{z}}\left(a_8\frac{\partial^2 u_x}{\partial t^2} + a_9\frac{\partial u_x}{\partial t} + a_{10}u_x\right) = 0\end{aligned}. \tag{49}$$

Substituting Equation (37) into Equation (49) results in

$$\tilde{z}^{m_G}\frac{d^2F}{d\tilde{z}^2} + m_G\tilde{z}^{m_G-1}\frac{dF}{d\tilde{z}} + A(\omega)F = \frac{d}{d\tilde{z}}\left(\tilde{z}^{m_G}\frac{dF}{d\tilde{z}}\right) + A(\omega)F = 0. \tag{50}$$

According to Courant and Hilbert[38], Equation (50) is classified as a Sturm-Liouville-type

differential equation (or Emden-Fowler-type equation), and its solution can be given by

$$F\left(\tilde{z}\right)=c_5F_1\left(\tilde{z}\right)+c_6F_2\left(\tilde{z}\right) \tag{51}$$

with

$$\begin{aligned}F_1\left(\tilde{z}\right)=&\left(\frac{2}{m_G}-1\right)^{\frac{1-m_G}{m_G-2}}m_G^{\frac{1-m_G}{m_G-2}}A^{\frac{m_G-1}{2(m_G-2)}}\left(\tilde{z}^{m_G}\right)^{\frac{1}{2(1/m_G-1)}}\\&\times\Gamma\left(\frac{1}{2-m_G}\right)J_{\frac{1-m_G}{m_G-2}}\left(-\frac{2\sqrt{A}\left(\tilde{z}^{m_G}\right)^{\frac{1}{m_G}-\frac{1}{2}}}{m_G-2}\right)\end{aligned} \tag{52}$$

$$\begin{aligned}F_2\left(\tilde{z}\right)=&\left(\frac{2}{m_G}-1\right)^{\frac{1-m_G}{m_G-2}}m_G^{\frac{1-m_G}{m_G-2}}A^{\frac{m_G-1}{2(m_G-2)}}\left(\tilde{z}^{m_G}\right)^{\frac{1}{2(1/m_G-1)}}\\&\times\Gamma\left(\frac{2m_G-3}{m_G-2}\right)J_{\frac{m_G-1}{m_G-2}}\left(-\frac{2\sqrt{A}\left(\tilde{z}^{m_G}\right)^{\frac{1}{m_G}-\frac{1}{2}}}{m_G-2}\right)\end{aligned} \tag{53}$$

where $c_i\left(i=5,6\right)$ are coefficients to be determined depending on boundary conditions, and $\Gamma\left(\bullet\right)$ is the Gamma function. When m_G is set to 0.5 for sandy materials[18], Equations (52) and (53) can be reduced to

$$F_1\left(\tilde{z}\right)=\sqrt[3]{\frac{2}{3}}\sqrt[6]{A}\sqrt[4]{\tilde{z}}\Gamma\left(\frac{2}{3}\right)J_{-\frac{1}{3}}\left(\frac{4}{3}\sqrt{A}\tilde{z}^{3/4}\right) \tag{54}$$

$$F_2\left(\tilde{z}\right)=\sqrt[3]{\frac{2}{3}}\sqrt[6]{A}\sqrt[4]{\tilde{z}}\Gamma\left(\frac{4}{3}\right)J_{\frac{1}{3}}\left(\frac{4}{3}\sqrt{A}\tilde{z}^{3/4}\right) \tag{55}$$

Substituting Equation (51) into Equation (37) produces the displacement solution of the solid skeleton under horizontal cyclic loading as

$$u_x\left(\tilde{z},t\right)=\left[c_5F_1\left(\tilde{z}\right)+c_6F_2\left(\tilde{z}\right)\right]\exp\left(i\omega t\right) \tag{56}$$

Then, the shear strain can be calculated by the partial differentiation of Equation (56) with $\tilde{z}$, as expressed below.

$$\frac{\partial u_x(\tilde{z},t)}{\partial \tilde{z}} = \left[c_5 \frac{dF_1(\tilde{z})}{d\tilde{z}} + c_6 \frac{dF_2(\tilde{z})}{d\tilde{z}} \right] \exp(i\omega t) \tag{57}$$

with

$$\frac{dF_1(\tilde{z})}{d\tilde{z}} = \left(\frac{2}{m_G} - 1 \right)^{\frac{1-m_G}{m_G-2}} m_G^{\frac{1-m_G}{m_G-2}} A^{\frac{m_G-1}{2(m_G-2)}} \Gamma\left(\frac{1}{2-m_G} \right) \frac{d\tilde{F}_1(\tilde{z})}{d\tilde{z}} \tag{58}$$

$$\begin{aligned} \frac{d\tilde{F}_1(\tilde{z})}{d\tilde{z}} = & \frac{m_G \tilde{z}^{m_G-1} \left(\tilde{z}^{m_G} \right)^{\frac{1}{2(1/m_G-1)}-1} J_{\frac{1-m_G}{m_G-2}} \left(-\frac{2\sqrt{A}\left(\tilde{z}^{m_G} \right)^{\frac{1}{m_G}-\frac{1}{2}}}{m_G-2} \right)}{2\left(\frac{1}{m_G} - 1 \right)} \\ & - \frac{1}{m_G-2} \sqrt{A} \left(\frac{1}{m_G} - \frac{1}{2} \right) m_G \tilde{z}^{m_G-1} \left(\tilde{z}^{m_G} \right)^{\frac{1}{m_G}+\frac{1}{2(1/m_G-1)}-\frac{3}{2}} \\ & \times \left[J_{\frac{1-m_G}{m_G-2}-1} \left(-\frac{2\sqrt{A}\left(\tilde{z}^{m_G} \right)^{\frac{1}{m_G}-\frac{1}{2}}}{m_G-2} \right) - J_{\frac{1-m_G}{m_G-2}+1} \left(-\frac{2\sqrt{A}\left(\tilde{z}^{m_G} \right)^{\frac{1}{m_G}-\frac{1}{2}}}{m_G-2} \right) \right] \end{aligned} \tag{59}$$

$$\frac{dF_2(\tilde{z})}{d\tilde{z}} = \left(\frac{2}{m_G} - 1 \right)^{\frac{1-m_G}{m_G-2}} m_G^{\frac{1-m_G}{m_G-2}} A^{\frac{m_G-1}{2(m_G-2)}} \Gamma\left(\frac{2m_G-3}{m_G-2} \right) \frac{d\tilde{F}_2(\tilde{z})}{d\tilde{z}} \tag{60}$$

$$\begin{aligned} \frac{d\tilde{F}_2(\tilde{z})}{d\tilde{z}} = & \frac{m_G \tilde{z}^{m_G-1} \left(\tilde{z}^{m_G} \right)^{\frac{1}{2(1/m_G-1)}-1} J_{\frac{m_G-1}{m_G-2}} \left(-\frac{2\sqrt{A}\left(\tilde{z}^{m_G} \right)^{\frac{1}{m_G}-\frac{1}{2}}}{m_G-2} \right)}{2\left(\frac{1}{m_G} - 1 \right)} \\ & - \frac{1}{m_G-2} \sqrt{A} \left(\frac{1}{m_G} - \frac{1}{2} \right) m_G \tilde{z}^{m_G-1} \left(\tilde{z}^{m_G} \right)^{\frac{1}{m_G}+\frac{1}{2(1/m_G-1)}-\frac{3}{2}} \\ & \times \left[J_{\frac{m_G-1}{m_G-2}-1} \left(-\frac{2\sqrt{A}\left(\tilde{z}^{m_G} \right)^{\frac{1}{m_G}-\frac{1}{2}}}{m_G-2} \right) - J_{\frac{m_G-1}{m_G-2}+1} \left(-\frac{2\sqrt{A}\left(\tilde{z}^{m_G} \right)^{\frac{1}{m_G}-\frac{1}{2}}}{m_G-2} \right) \right] \end{aligned} \tag{61}$$

When m_G is set to 0.5, Equations (58) and (60) can be reduced to

$$\frac{dF_1(\tilde{z})}{d\tilde{z}} = \frac{A^{2/3}\Gamma\left(\frac{2}{3}\right)\left[J_{-\frac{4}{3}}\left(\frac{4}{3}\sqrt{A}\tilde{z}^{3/4}\right) - J_{\frac{2}{3}}\left(\frac{4}{3}\sqrt{A}\tilde{z}^{3/4}\right)\right]}{2^{2/3}\sqrt[3]{3}} + \frac{\sqrt[6]{A}\Gamma\left(\frac{2}{3}\right)J_{-\frac{1}{3}}\left(\frac{4}{3}\sqrt{A}\tilde{z}^{3/4}\right)}{2^{5/3}\sqrt[3]{3}\tilde{z}^{3/4}} \tag{62}$$

$$\frac{dF_2(\tilde{z})}{d\tilde{z}} = \frac{A^{2/3}\Gamma\left(\frac{4}{3}\right)\left[J_{-\frac{2}{3}}\left(\frac{4}{3}\sqrt{A}\tilde{z}^{3/4}\right) - J_{\frac{4}{3}}\left(\frac{4}{3}\sqrt{A}\tilde{z}^{3/4}\right)\right]}{2^{2/3}\sqrt[3]{3}} + \frac{\sqrt[6]{A}\Gamma\left(\frac{4}{3}\right)J_{\frac{1}{3}}\left(\frac{4}{3}\sqrt{A}\tilde{z}^{3/4}\right)}{2^{5/3}\sqrt[3]{3}\tilde{z}^{3/4}} \tag{63}$$

The coefficients $c_i\left(i=5,6\right)$ in Equations (56) and (57) can be obtained under appropriate boundary conditions: Equations (28) and (29) for the ground surface stress loading (Fig. 3(a)); Equations (30) and (31) for the bottom displacement loading (Fig. 3(b)).

By solving Equations (48) and (22) for the average relative fluid displacement, $\overline{w}_x$ is found to take a similar form as the soil skeleton displacement u_x (see Equation (56)), as expressed below.

$$\overline{w}_x\left(\tilde{z},t\right) = \left[c_5\eta_5 F_1\left(\tilde{z}\right) + c_6\eta_6 F_2\left(\tilde{z}\right)\right]\exp\left(i\omega t\right). \tag{64}$$

The coefficients $\eta_i\left(i=5,6\right)$ can be derived by substituting Equations (56) and (64) into Equation (48) as

$$\eta_5 = -\frac{\mu_{\text{ref}} + i\omega\mu'_{\text{ref}}}{\rho_f\omega^2 F_1\left(\tilde{z}\right)}\left(\frac{\tilde{z}}{\tilde{z}_{\text{ref}}}\right)^{m_G}\left[\frac{d^2F_1\left(\tilde{z}\right)}{d\tilde{z}^2} + \frac{m_G}{\tilde{z}}\frac{dF_1\left(\tilde{z}\right)}{d\tilde{z}}\right] - \frac{\rho}{\rho_f}. \tag{65}$$

$$\eta_6 = -\frac{\mu_{\text{ref}} + i\omega\mu'_{\text{ref}}}{\rho_f\omega^2 F_2\left(\tilde{z}\right)}\left(\frac{\tilde{z}}{\tilde{z}_{\text{ref}}}\right)^{m_G}\left[\frac{d^2F_2\left(\tilde{z}\right)}{d\tilde{z}^2} + \frac{m_G}{\tilde{z}}\frac{dF_2\left(\tilde{z}\right)}{d\tilde{z}}\right] - \frac{\rho}{\rho_f}. \tag{66}$$

4. NUMERICAL CALCULATION UNDER HORIZONTAL STRESS LOADING AT THE GROUND SURFACE

This section numerically investigates the dynamic response of a viscoelastic soil column subjected to horizontal stress loading at the ground surface (Fig. 3(a)). The soil parameters used in the numerical calculation are listed in Table 1. The bulk moduli $K_i\left(i=b,s,w,a\right)$ and the degree of saturation S_r were not specified because they do not affect the horizontal vibration response (e.g., Equations (21) and (22)). The Lame elastic modulus μ_{ref} at depth z_{ref} for Types B and C ($m_G=0.5$) was set to the same value as the depth-independent constant modulus for Type A. Based on the reference modulus μ_{ref} and the model parameter z_0, the shear wave velocity profiles (solid lines) shown in Fig. 4 were calculated from $V_{\text{s}}=\sqrt{\mu/\rho}$ using the distribution of $\mu(z)$ (dotted lines) given by Equations (13) and (18) for Types B and C, respectively; the depth profiles for $z_0=10^{-10}$ m and $z_0=10^{-2}$ m are almost overlapping. The retardation time τ was assumed to be 0.00 (i.e., poroelastic), 0.01, 0.05, and 0.10 s to investigate the viscous damping effect on the response; according to Equation (7), the values cover the damping ratio range under a machine foundation vibration and seismic loading[39-41]. The permeability coefficient was set as constant (10^{-3} m/s) in this study because varying the coefficient between 10^{-2} m/s and 10^{-9} m/s has minimal effect on the horizontal vibration compared to a change in the retardation time, as shown by Chen et al.[22] for Type A. When the Lame elastic modulus μ depends on depth (for Types B and C), the reference depth

z_{ref} in Equations (13) and (18) was set to achieve the same first resonance frequency as Type A under the condition of the model parameters μ_{ref} and z_0 listed in Table 1. For example, by substituting $K_0 = 0.5$ and $\phi'_{\text{f}} = 37.7°$ into Equation (15), $z_0 = 10^0$ m and $z_0 = 10^1$ m correspond to 5 kPa and 50 kPa of soil cohesion, respectively.

4.1. Dynamic response at the ground surface

Fig. 5 shows the displacement amplitude at the ground surface, which is subjected to horizontal (or shear) stress (Fig. 3(a)), versus loading frequency when the Lame elastic and loss moduli, μ and μ', are assumed to be depth-independent (i.e., Type A). The horizontal displacement is normalized with $u_s = \tau_0 L / \mu$, which denotes the maximum shear displacement at the ground surface that is subjected to static loading, to express the amplification factor on the graph's vertical axis. As examined by Chen et al.[22], the retardation time τ (or viscous damping) of soil is found to have a significant attenuation effect on the dynamic response except in a region where the frequency is close to 0 Hz.

Before examining the dynamic response of a viscoelastic soil column for Types B and C, we may have to verify that the derivation of the analytical solutions is correct because it is not easy to trace the derivation process due to the existence of Bessel and Gamma functions. Here, cross-validation will be performed by comparing the analytical solutions and corresponding numerical simulation results, although it is standard practice to use an analytical solution as a correct one to validate numerical simulation. The present results of the amplification factor at the soil surface for Types B and C ($m_G = 0.5$) with $z_0 = 10^0$ m are shown by solid lines in Fig. 6, compared with the simulation results

(circle plots) using a finite element computer program named "FLIP ROSE"[42-44]. Note that the program is capable of considering the governing equations and constitutive models described in Section 2. In the simulation, the depth-dependent Lame elastic modulus in Fig. 4 was set for a soil column model consisting of 60 elements to calculate the steady-state response under harmonic loading with different frequencies at the ground surface. The agreement between both results demonstrates the validity of the analytical solutions as well as that of the numerical simulation.

When the Lame elastic and loss moduli are linearly dependent on depth (i.e., Type B), the variation of the amplification factor versus frequency is illustrated in Fig. 7. It is worth noting that μ_{ref} is used, instead of μ, for calculating the maximum shear displacement $u_s \left(= \tau_0 L / \mu_{\text{ref}}\right)$. As an overall trend, comparing the same z_0 conditions demonstrates that the dynamic response changes from periodic (or oscillatory) to aperiodic (or over-damped) as the retardation time τ increases, which is similar to Type A. Next, let us consider the effect of z_0, which corresponds to soil cohesion. When τ is large and the dynamic response is aperiodic (see Fig. 7(c)(d)), the increase in z_0 has a different influence on the amplification factor depending on the loading frequency; the amplification factor becomes slightly larger for the normalized frequency f / f_1 below 1.2, whereas it becomes smaller for f / f_1 above 1.2. When the dynamic response is periodic, as shown in Fig. 7(a), it can be demonstrated that the value of z_0 affects not only the displacement amplitude at each peak (or valley) but also the phase characteristic; as z_0 (or soil cohesion) increases, the amplitude decay tends to be suppressed and the peak-to-peak period to be elongated. When z_0 is approximately zero, it seems to repeat

small oscillations around the amplification factor of 1.0 even in a high-frequency region. Note that if z_0 is set to zero, the calculation cannot be performed for the surface stress loading because the Lame moduli at the ground surface become zero (see Equation (13)).

Fig. 8 depicts the variation of the amplification factor for Type C ($m_G = 0.5$), in which the Lame moduli are nonlinearly dependent on depth. Similar to Type B, the horizontal displacement is normalized with $u_s = \tau_0 L / \mu_{\text{ref}}$. As the retardation time τ increases, the transition from a periodic to an aperiodic response is observed, which is similar to Types A and B. When the dynamic response is aperiodic with τ greater than 0.05 (see Fig. 8(c)(d)), the effect of z_0 on the amplification factor is found to be not as large as that of Type B shown in Fig. 7(c)(d). Meanwhile, it can be seen that the dynamic periodic response of poroelastic media (i.e., $\tau = 0$) in Fig. 8(a) is greatly affected by the parameter z_0; the peak-to-peak period is elongated as z_0 increases. It is worth noting that the difference between the amplification factors with $z_0 = 10^{-10}$ m and $z_0 = 10^{-2}$ m is hardly observed in Fig. 8(a), compared to Type B in Fig. 7(a), because the shear moduli near the ground surface for Type C is greater than that for Type B, as shown in Fig. 1.

4.2. Effect of the depth dependency of material dynamic properties

Fig. 9 compares the effect of the Lame moduli's depth-dependency on the dynamic response at the ground surface subjected to horizontal stress loading; four cases are presented in the figure, depending on the combination of $\tau\left(= 0.00, 0.01 \text{ s}\right)$ and $z_0\left(= 10^{-2}, 10^{1} \text{ m}\right)$ listed in Table 1. While the elastic aperiodic responses in Fig. 9(b) make a difference among the three types, particularly after the first resonance frequency,

the viscoelastic ones in Fig. 9(d) are almost unaffected by the depth-dependency. When the dynamic response is periodic, as shown in Fig. 9(a)(c), it can be seen that the peak-to-peak period is shorter for Type C than for Type A and for Type B than for Type C, even though the depth-dependency effect is slightly smaller in poro-viscoelastic media.

The amplification factor distributions with depth under the ground surface horizontal stress loading are illustrated in Fig. 10 (for $z_0 = 10^{-2}$ m) and Fig. 11 (for $z_0 = 10^{1}$ m); in these figures, the effect of the Lame moduli's depth-dependency is compared, along with the retardation time effect. Fig. 10(a) and Fig. 11(a) indicate that the poroelastic soil column shows a large amplification toward the ground surface, compared to the poro-viscoelastic soil column, at the first resonance frequency. In addition, it is found that the depth profile shape (or the slope in the depth direction) is greatly affected by the Lame moduli's depth dependency, along with the retardation time. In particular, for poroelastic media, the depth distribution becomes more complex as the loading frequency increases.

5. NUMERICAL CALCULATION UNDER HORIZONTAL DISPLACEMENT LOADING AT THE GROUND BOTTOM

In this section, the dynamic response of a viscoelastic soil column that is subjected to horizontal displacement loading at the ground bottom is numerically studied. Except for the boundary conditions shown in Fig. 3(b), the model parameters used in the calculation are the same as in the previous section (see Table 1).

5.1. Dynamic response at the ground surface

Fig. 12 shows the displacement amplitude at the ground surface versus loading

frequency when a soil column with depth-independent material properties (i.e., Type A) is subjected to horizontal cyclic displacement loading at the bottom. The horizontal displacement is normalized with $u_s = u_0$, which denotes the bottom displacement amplitude. The figure demonstrates that the dynamic response changes from periodic to aperiodic as τ increases; for poroelastic media, the amplification factor is always greater than 1.0, regardless of frequency, whereas for poro-viscoelastic media, the amplitude attenuates significantly in a large frequency range.

When the Lame moduli are linearly dependent on depth (i.e., Type B), the variation of the amplification factor versus frequency is depicted in Fig. 13. As an overall trend, comparing the same z_0 condition demonstrates that the dynamic response changes from periodic to aperiodic as the retardation time τ increases, which is similar to Type A. When τ is large and the dynamic response is aperiodic (see Fig. 13(c)(d)), the influence of the cohesion-related parameter z_0 is trivial and no significant difference is found in the amplification factor. However, when the material is poroelastic and the dynamic response is periodic, Fig. 13(a) shows that the value of z_0 affects not only the displacement amplitude but also the phase characteristic; as z_0 increases, the amplitudes at the corresponding peaks (or valleys) tend to be smaller and the peak-to-peak period to be elongated.

Fig. 14 illustrates the variation of the amplification factor for Type C ($m_G = 0.5$), in which the Lame moduli are nonlinearly dependent on depth. Similar to Type B, the dynamic aperiodic response in Fig. 14(c)(d) is almost unaffected by the cohesion-related parameter z_0. Meanwhile, the dynamic periodic response of poroelastic media is influenced by z_0; the amplitudes at corresponding peaks (or valleys) slightly decrease

and the peak-to-peak period becomes longer as z_0 increases.

5.2. Effect of the depth-dependency of material dynamic properties

Fig. 15 compares the effect of the Lame moduli's depth-dependency on the ground surface dynamic response of poroelastic and poro-viscoelastic soil columns subjected to the bottom displacement loading; four cases are presented in the figure, depending on the combination of $\tau\left(=0.00, 0.01\ \mathrm{s}\right)$ and $z_0\left(=10^{-2}, 10^{1}\ \mathrm{m}\right)$ listed in Table 1. Compared to the difference among the elastic aperiodic responses for Types A, B, and C (see Fig. 15(b)), the depth-dependency effect is found to be minimal on the viscoelastic aperiodic response as shown in Fig. 15(d). When the dynamic response is periodic, the peak-to-peak period becomes shorter in the order of Types B, C, and A, to varying degrees between Fig. 15(a) and Fig. 15(d); in addition, the amplitudes at the corresponding peaks (or valleys) are largest for Type B and smallest for Type A.

The amplification factor distributions with depth under the ground bottom horizontal displacement loading are illustrated in Fig. 16 (for $z_0 = 10^{-2}$ m) and Fig. 17 (for $z_0 = 10^{1}$ m); in these figures, the effect of the Lame moduli's depth dependency is compared, along with the retardation time effect. Compared to the poro-viscoelastic soil column, the poroelastic soil column produces large amplification toward the ground surface at the first resonance frequency, as shown in Fig. 16(a) and Fig. 17(b). It is also demonstrated that the depth profile shape (or the slope in the depth direction) is greatly affected by the Lame moduli's depth-dependency, along with the retardation time. Particularly for poroelastic media, the depth distribution becomes more complex as the loading frequency increases, rather than the horizontal stress loading at the ground surface

(e.g., compare Fig. 16(d) with Fig. 11(d)).

6. CONCLUSIONS

In this paper, a series of analytical solutions were proposed on the dynamic response of a viscoelastic two-phase porous medium that is subjected to horizontal cyclic loading. To investigate the effect of the confining-pressure dependency of material dynamic properties (i.e., the Lame elastic and loss moduli), two types of soil profiles were adopted in addition to the constant stiffness with depth (Type A): stiffness linearly increasing with depth (Type B) and stiffness nonlinearly increasing with depth (Type C). The influences of loading frequency, retardation time (or viscous damping), and the newly introduced model parameter corresponding to soil cohesion (only for Types B and C) were numerically examined.

When a soil layer was subjected to the horizontal stress loading at the ground surface or to the horizontal displacement loading at the bottom, regardless of the soil profile type, a common trend was observed that the dynamic displacement amplitude at the ground surface versus loading frequency changed from periodic (or oscillatory) to aperiodic (or over-damped) as the retardation time increased. When the dynamic response was periodic, the peak-to-peak period became shorter and the amplitude at the corresponding peaks (or valleys) became larger in the order of Types B, C, and A. It was also demonstrated that the amplification factor distribution with depth is greatly affected by the Lame moduli's depth-dependency. However, the depth-dependency effect was found to be small on the viscoelastic aperiodic response.

The influence of cohesion-related parameter was small on the amplification factor when

the response was aperiodic, particularly for Type C. However, when the response is periodic, the parameter value was found to affect not only the displacement amplitude but also the phase characteristic; as the cohesion increased, the amplitudes at the corresponding peaks (or valleys) tended to be smaller and the peak-to-peak period to be elongated.

DATA AVAILABILITY STATEMENT

The data that support the findings of this study are available from the corresponding author (Kyohei Ueda) upon reasonable request.

REFERENCES

1. Hung HH, Yang YB. Elastic waves in visco-elastic half-space generated by various vehicle loads. *Soil Dynamics and Earthquake Engineering*. 2001;21(1):1-17. doi:https://doi.org/10.1016/S0267-7261(00)00078-6
2. Yang J, Yan XR. Factors affecting site response to multi-directional earthquake loading. *Engineering Geology*. 2009;107(3):77-87. doi:https://doi.org/10.1016/j.enggeo.2009.04.002
3. Ye JH, Jeng D-S. Response of Porous Seabed to Nature Loadings: Waves and Currents. *Journal of Engineering Mechanics*. 2012;138(6):601-613. doi:doi:10.1061/(ASCE)EM.1943-7889.0000356
4. Chen W-Y, Wang Z-H, Chen G-X, Jeng D-S, Wu M, Zhao H-Y. Effect of vertical seismic motion on the dynamic response and instantaneous liquefaction in a two-layer porous seabed. *Computers and Geotechnics*. 2018;99:165-176. doi:https://doi.org/10.1016/j.compgeo.2018.03.005
5. Zhang N, Zhang Y, Gao Y, Pak RYS, Wu Y, Zhang F. An exact solution for SH-wave scattering by a radially multilayered inhomogeneous semicylindrical canyon. *Geophysical Journal International*. 2019;217(2):1232-1260. doi:10.1093/gji/ggz083
6. Chen W, Jeng D, Chen W, Chen G, Zhao H. Seismic-induced dynamic responses in a poro-elastic seabed: Solutions of different formulations. *Soil Dynamics and Earthquake Engineering*. 2020/04/01/ 2020;131:106021. doi:https://doi.org/10.1016/j.soildyn.2019.106021
7. Zhang N, Zhang Y, Gao Y, Pak RYS, Yang J. Site amplification effects of a radially multi-layered semi-cylindrical canyon on seismic response of an earth and rockfill dam. *Soil Dynamics and Earthquake Engineering*. 2019;116:145-163. doi:https://doi.org/10.1016/j.soildyn.2018.09.014
8. Biot MA. Theory of Propagation of Elastic Waves in a Fluid‐Saturated Porous Solid. I. Low‐Frequency Range. *The Journal of the Acoustical Society of America*. 1956;28(2):168-178. doi:10.1121/1.1908239

9. Biot MA. General Theory of Three‐Dimensional Consolidation. *Journal of Applied Physics*. 1941;12(2):155-164. doi:10.1063/1.1712886
10. Biot MA. Generalized Theory of Acoustic Propagation in Porous Dissipative Media. *The Journal of the Acoustical Society of America*. 1962;34(9A):1254-1264. doi:10.1121/1.1918315
11. Biot MA. Mechanics of Deformation and Acoustic Propagation in Porous Media. *Journal of Applied Physics*. 1962;33(4):1482-1498. doi:10.1063/1.1728759
12. Simon BR, Zienkiewicz OC, Paul DK. An analytical solution for the transient response of saturated porous elastic solids. *International Journal for Numerical and Analytical Methods in Geomechanics*. 1984;8(4):381-398. doi:https://doi.org/10.1002/nag.1610080406
13. de Boer R, Ehlers W, Liu Z. One-dimensional transient wave propagation in fluid-saturated incompressible porous media. *Archive of Applied Mechanics*. 1993;63(1):59-72. doi:10.1007/BF00787910
14. Jun Y, Song EX, Chen ZY. Analytical solution of 1-D harmonic response in saturated soil. *Yantu Lixue/Rock and Soil Mechanics*. 08/01 2003;24:505-509.
15. Zienkiewicz OC, Chang CT, Bettess P. Drained, undrained, consolidating and dynamic behaviour assumptions in soils. *Géotechnique*. 1980;30(4):385-395. doi:10.1680/geot.1980.30.4.385
16. Zienkiewicz OC, Shiomi T. Dynamic behaviour of saturated porous media; The generalized Biot formulation and its numerical solution. *International Journal for Numerical and Analytical Methods in Geomechanics*. 1984;8(1):71-96. doi:https://doi.org/10.1002/nag.1610080106
17. Yang J, Sato T. Influence of viscous coupling on seismic reflection and transmission in saturated porous media. *Bulletin of the Seismological Society of America*. 1998;88(5):1289-1299.
18. Ishihara K. *Soil Behaviour in Earthquake Geotechnics*. Clarendon Press; 1996.
19. Bardet JP. A Viscoelastic Model for the Dynamic Behavior of Saturated Poroelastic Soils. *Journal of Applied Mechanics*. 1992;59(1):128-135. doi:10.1115/1.2899417
20. Militano G, Rajapakse RKND. Dynamic response of a pile in a multi-layered soil to transient torsional and axial loading. *Géotechnique*. 1999;49(1):91-109. doi:10.1680/geot.1999.49.1.91
21. Xie K-h, Liu G-b, Shi Z-y. Dynamic response of partially sealed circular tunnel in viscoelastic saturated soil. *Soil Dynamics and Earthquake Engineering*. 2004/12/01/ 2004;24(12):1003-1011. doi:https://doi.org/10.1016/j.soildyn.2004.05.005
22. Chen W, Mou Y, Xu L, Wang Z, Luo J. Frequency-dependent dynamic behavior of a poroviscoelastic soil layer under cyclic loading. *International Journal for Numerical and Analytical Methods in Geomechanics*. 2020;44(9):1336-1349. doi:https://doi.org/10.1002/nag.3064
23. Hardin BO, Drnevich VP. Shear Modulus and Damping in Soils: Design Equations and Curves. *Journal of the Soil Mechanics and Foundations Division*. 1972;98(7):667-692. doi:doi:10.1061/JSFEAQ.0001760
24. Seed HB, Wong RT, Idriss IM, Tokimatsu K. Moduli and Damping Factors for Dynamic Analyses of Cohesionless Soils. *Journal of Geotechnical Engineering*. 1986;112(11):1016-1032. doi:doi:10.1061/(ASCE)0733-9410(1986)112:11(1016)
25. Kokusho T, Yoshida Y, Esashi Y. Dynamic Properties of Soft Clay for Wide Strain Range. *Soils and Foundations*. 1982/12/01/ 1982;22(4):1-18. doi:https://doi.org/10.3208/sandf1972.22.4_1
26. Ishibashi I, Zhang X. Unified Dynamic Shear Moduli and Damping Ratios of Sand and Clay. *Soils and Foundations*. 1993/03/01/ 1993;33(1):182-191. doi:https://doi.org/10.3208/sandf1972.33.182
27. Jeng D-S, Shown Lin Y. Finite element modelling for water waves-soil interaction. *Soil Dynamics and Earthquake Engineering*. 1996/07/01/ 1996;15(5):283-300.

doi:https://doi.org/10.1016/0267-7261(96)00009-7
28. Yeh CH, Rahman MS. Stochastic finite element methods for the seismic response of soils. *International Journal for Numerical and Analytical Methods in Geomechanics*. 1998;22(10):819-850. doi:https://doi.org/10.1002/(SICI)1096-9853(1998100)22:10<819::AID-NAG943>3.0.CO;2-I
29. Zhang LL, Cheng Y, Li JH, Zhou XL, Jeng DS, Peng XY. Wave-induced oscillatory response in a randomly heterogeneous porous seabed. *Ocean Engineering*. 2016/01/01/ 2016;111:116-127. doi:https://doi.org/10.1016/j.oceaneng.2015.10.016
30. Cheng Z, Leong EC. Finite element simulations of wave propagation in soils using a Viscoelastic model. *Soil Dynamics and Earthquake Engineering*. 2016/09/01/ 2016;88:207-214. doi:https://doi.org/10.1016/j.soildyn.2016.06.005
31. Sills GC, Wheeler SJ, Thomas SD, Gardner TN. Behaviour of offshore soils containing gas bubbles. *Géotechnique*. 1991;41(2):227-241. doi:10.1680/geot.1991.41.2.227
32. Verruijt A. Elastic storage of aquifers. In" Flow through Porous Media", edited by RJM DeWiest. Academic Press, New York; 1969.
33. Yamamoto T, Koning H, Sellmeijer H, Van Hijum E. On the response of a poro-elastic bed to water waves. *Journal of Fluid Mechanics*. 1978;87(1):193-206.
34. Pietruszczak S, Pande GN. Constitutive Relations for Partially Saturated Soils Containing Gas Inclusions. *Journal of Geotechnical Engineering*. 1996;122(1):50-59. doi:doi:10.1061/(ASCE)0733-9410(1996)122:1(50)
35. Dakoulas P, Gazetas G. A class of inhomogeneous shear models for seismic response of dams and embankments. *International Journal of Soil Dynamics and Earthquake Engineering*. 1985/10/01/ 1985;4(4):166-182. doi:https://doi.org/10.1016/0261-7277(85)90037-3
36. Towhata I. Seismic Wave Propagation in Elastic Soil With Continuous Variation of Shear Modulus in the Vertical Direction. *Soils and Foundations*. 1996/03/01/ 1996;36(1):61-72. doi:https://doi.org/10.3208/sandf.36.61
37. Travasarou T, Gazetas G. On the Linear Seismic Response of Soils With Modulus Varying as a Power of Depth-The Maliakos Marine Clay. *Soils and Foundations*. 2004/10/01/ 2004;44(5):85-93. doi:https://doi.org/10.3208/sandf.44.5_85
38. Courant R, Hilbert D. Vibration and Eigenvalue Problems. *Methods of Mathematical Physics*. 1989:275-396.
39. Veletsos AS, Verbič B. Vibration of viscoelastic foundations. *Earthquake Engineering & Structural Dynamics*. 1973;2(1):87-102. doi:https://doi.org/10.1002/eqe.4290020108
40. Jongmans D. In-situ attenuation measurements in soils. *Engineering Geology*. 1990/07/01/ 1990;29(2):99-118. doi:https://doi.org/10.1016/0013-7952(90)90001-H
41. Gibbs JF, Boore DM, Joyner WB, Fumal TE. The attenuation of seismic shear waves in quaternary alluvium in Santa Clara Valley, California. *Bulletin of the Seismological Society of America*. 1994;84(1):76-90.
42. Vargas RR, Ueda K, Tobita T. Centrifuge modeling of the dynamic response of a sloping ground – LEAP-UCD-2017 and LEAP-ASIA-2019 tests at Kyoto University. *Soil Dynamics and Earthquake Engineering*. 2021;140doi:10.1016/j.soildyn.2020.106472
43. Ueda K, Uzuoka R, Iai S, Okamura T. Centrifuge model tests and effective stress analyses of offshore wind turbine systems with a suction bucket foundation subject to seismic load. *Soils and Foundations*. 2020;60(6):1546-1569. doi:10.1016/j.sandf.2020.08.007
44. Ueda K, Iai S. Numerical Predictions for Centrifuge Model Tests of a Liquefiable Sloping Ground Using a Strain Space Multiple Mechanism Model Based on the Finite Strain Theory. *Soil Dynamics and Earthquake Engineering*. 2018;113:771-792. doi:10.1016/j.soildyn.2016.11.015

Figure Legends

Fig. 1 Plots of the Lame elastic modulus versus depth: (a) constant stiffness with depth (Type A); (b) stiffness linearly increasing with depth (Type B); (c) stiffness nonlinearly increasing with depth (Type C)

Fig. 2 Generalized Kelvin–Voigt model

Fig. 3 Geometry and boundary conditions of a soil column that is subjected to horizontal loading: (a) stress loading at the ground surface, (b) displacement loading at the bottom

Fig. 4 Depth profile of the Lame elastic modulus μ and shear wave velocity: (a) Type B, (b) Type C ($m_G = 0.5$)

Fig. 5 Effect of retardation time on the dynamic response at the ground surface under the horizontal stress loading at the ground surface for Type A

Fig. 6 Comparison of the amplification factor at the ground surface between the present study and FEM simulation: (a) Type B with $z_0 = 10^0$ m, (b) Type C with $z_0 = 10^0$ m

Fig. 7 Effect of the parameter z_0 on the dynamic response at the ground surface under the horizontal stress loading at the ground surface for Type B with a different retardation time: (a) $\tau = 0.00$ (poroelastic), (b) $\tau = 0.01$, (c) $\tau = 0.05$, (d) $\tau = 0.10$

Fig. 8 Effect of the parameter z_0 on the dynamic response at the ground surface under the horizontal stress loading at the ground surface for Type C ($m_G = 0.5$) with a different retardation time: (a) $\tau = 0.00$ (poroelastic), (b) $\tau = 0.01$, (c) $\tau = 0.05$, (d) $\tau = 0.10$

Fig. 9 Effect of the Lame moduli's depth dependency on the dynamic response at the ground surface under the horizontal stress loading at the ground surface: (a) $\tau = 0.00$ (poroelastic) with $z_0 = 10^{-2}$ m, (b) $\tau = 0.01$ with $z_0 = 10^{-2}$ m, (c) $\tau = 0.00$ (poroelastic) with $z_0 = 10^1$ m, (d) $\tau = 0.01$ with $z_0 = 10^1$ m

Fig. 10 Effect of the Lame moduli's depth dependency and retardation time on the dynamic response depth profile under the horizontal stress loading at the ground surface ($z_0 = 10^{-2}$ m) at a different frequency: (a) $f/f_1 = 1.0$, (b) $f/f_1 = 1.5$, (c) $f/f_1 = 2.0$, (d) $f/f_1 = 2.5$, where f_1 is the first resonance frequency

Fig. 11 Effect of the Lame moduli's depth dependency and retardation time on the dynamic response depth profile under the horizontal stress loading at the ground surface ($z_0 = 10^1$ m) at a different frequency: (a) $f/f_1 = 1.0$, (b) $f/f_1 = 1.5$, (c) $f/f_1 = 2.0$, (d) $f/f_1 = 2.5$, where f_1 is the first resonance frequency

Fig. 12 Effect of retardation time on the dynamic response at the ground surface under the horizontal bottom displacement loading for Type A

Fig. 13 Effect of the parameter z_0 on the dynamic response at the ground surface under the horizontal bottom displacement loading for Type B with a different retardation time: (a) $\tau = 0.00$ (poroelastic), (b) $\tau = 0.01$, (c) $\tau = 0.05$, (d) $\tau = 0.10$

Fig. 14 Effect of the parameter z_0 on the dynamic response at the ground surface under the horizontal bottom displacement loading for Type C with a different retardation time: (a) $\tau = 0.00$ (poroelastic), (b) $\tau = 0.01$, (c) $\tau = 0.05$, (d) $\tau = 0.10$

Fig. 15 Effect of the Lame moduli's depth dependency on the dynamic response at the ground surface under the horizontal bottom displacement loading: (a) $\tau = 0.00$ (poroelastic) with $z_0 = 10^{-2}$ m, (b) $\tau = 0.01$ with $z_0 = 10^{-2}$ m, (c) $\tau = 0.00$ (poroelastic) with $z_0 = 10^1$ m, (d) $\tau = 0.01$ with $z_0 = 10^1$ m

Fig. 16 Effect of the Lame moduli's depth dependency and retardation time on the dynamic response depth profile under the horizontal bottom displacement loading

($z_0 = 10^{-2}$ m) at a different frequency: (a) $f/f_1 = 1.0$, (b) $f/f_1 = 1.5$, (c) $f/f_1 = 2.0$, (d) $f/f_1 = 2.5$, where f_1 is the first resonance frequency

Fig. 17 Effect of the Lame moduli's depth dependency and retardation time on the dynamic response depth profile under the horizontal bottom displacement loading ($z_0 = 10^1$ m) at a different frequency: (a) $f/f_1 = 1.0$, (b) $f/f_1 = 1.5$, (c) $f/f_1 = 2.0$, (d) $f/f_1 = 2.5$, where f_1 is the first resonance frequency

Table 1. Soil properties used in the computation.

Parameter	Notation	Value
Thickness of soil column	L	30 m
Density of solid particle	ρ_s	2,650 kg/m^3
Density of water	ρ_f	1,000 kg/m^3
Porosity	n	0.4
Permeability	k_f	10^{-3} m/s
Bulk modulus of the solid skeleton	K_b	Not used
Bulk modulus of solid particle	K_s	Not used
Bulk modulus of water	K_w	Not used
Bulk modulus of air	K_a	Not used
Degree of saturation	S_r	Not used
Retardation time	τ	0.00, 0.01, 0.05, 0.10 s
Lame elastic modulus (for Type A)	μ	79.6 MPa
Lame elastic modulus at depth z_{ref} (for Types B and C)	μ_{ref}	79.6 MPa
Reference depth (for Types B and C)	z_{ref}	Set to have the same first resonance frequency as Type A
Model parameter corresponding to soil cohesion (for Types B and C)	z_0	10^{-10}, 10^{-2}, 10^{0}, 10^{1} m

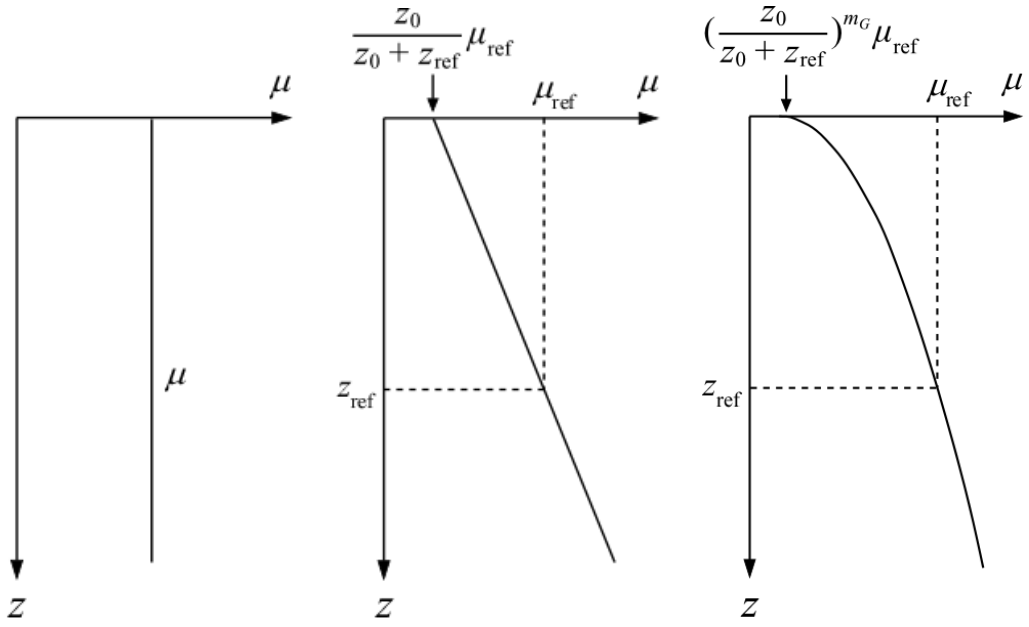

(a) (b) (c)

Figure 1. Plots of the Lame elastic modulus versus depth: (a) constant stiffness with depth (Type A); (b) stiffness linearly increasing with depth (Type B); (c) stiffness nonlinearly increasing with depth (Type C)

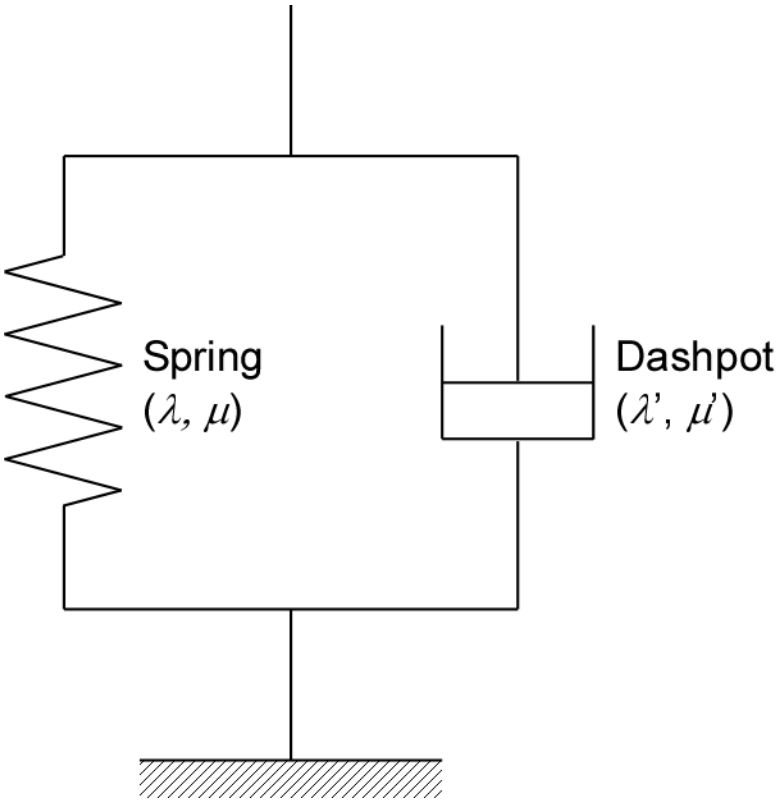

Figure 2. Generalized Kelvin–Voigt model

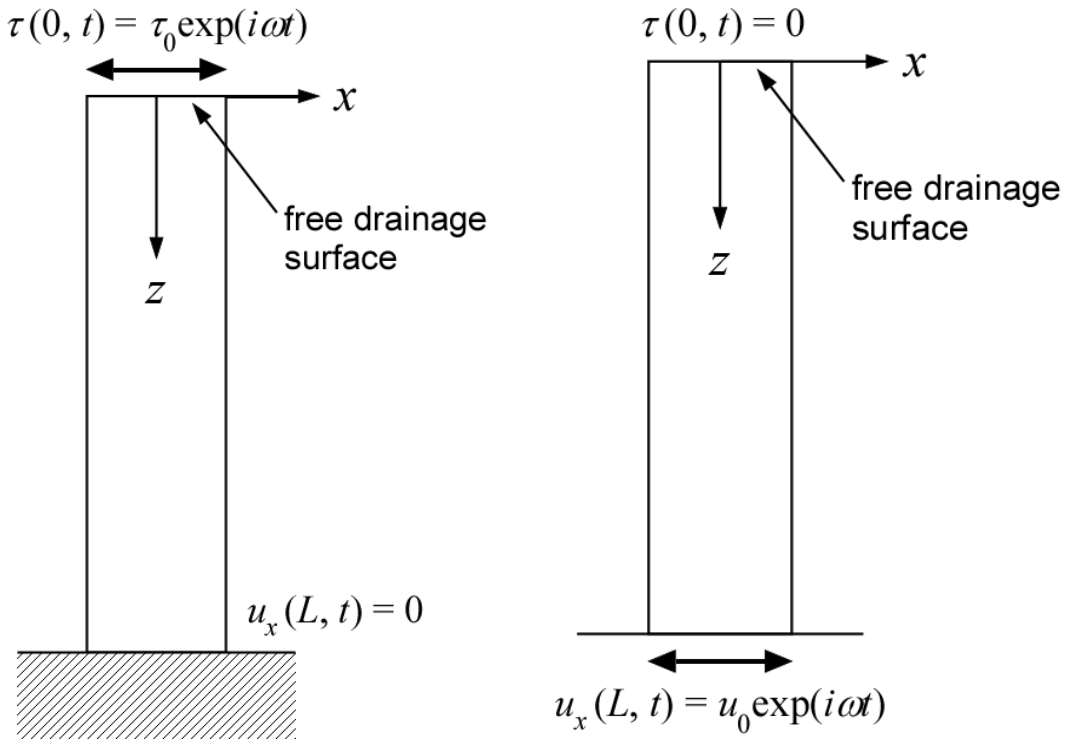

(a) (b)

Figure 3. Geometry and boundary conditions of a soil column that is subjected to horizontal loading: (a) stress loading at the ground surface, (b) displacement loading at the bottom

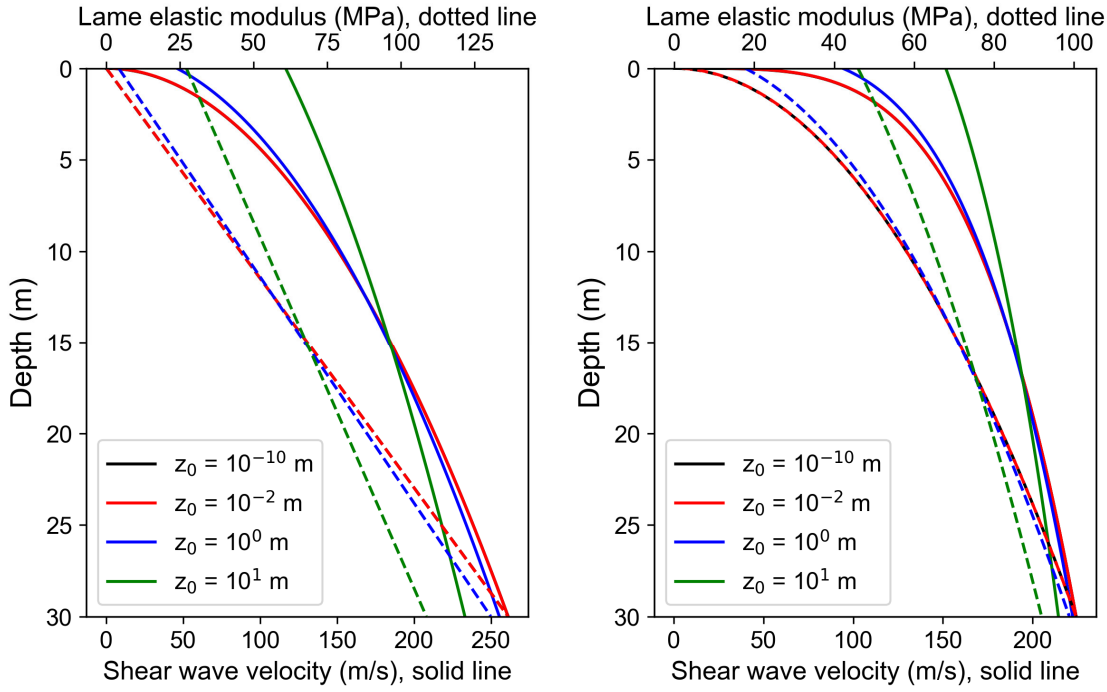

(a) (b)

Figure 4. Depth profile of the Lame elastic modulus μ and shear wave velocity: (a) Type B, (b) Type C ($m_G = 0.5$)

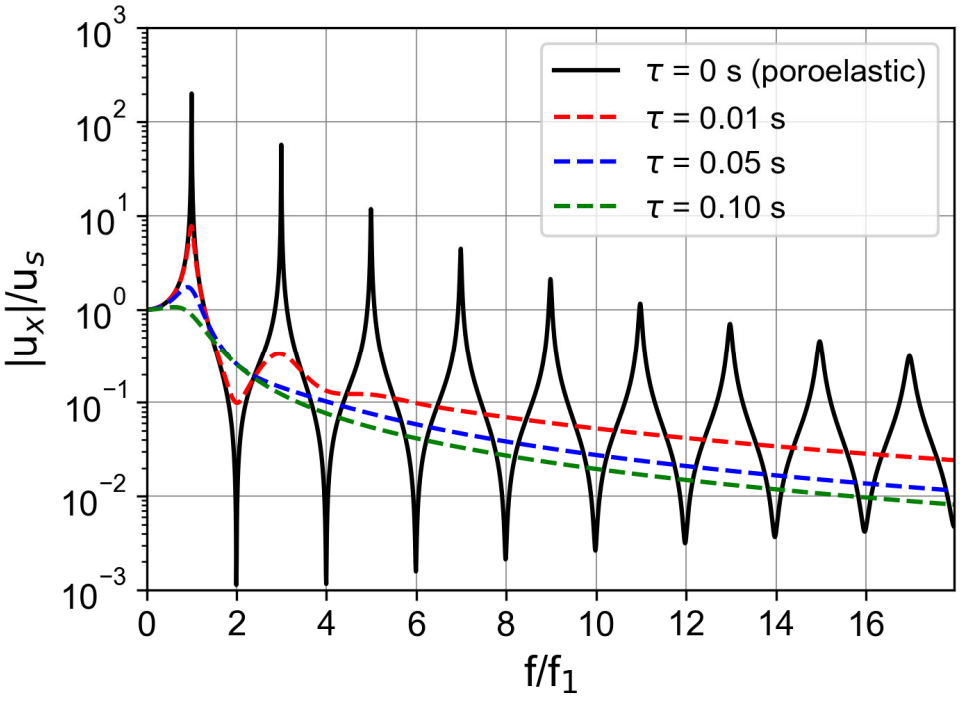

Figure 5. Effect of retardation time on the dynamic response at the ground surface under the horizontal stress loading at the ground surface for Type A

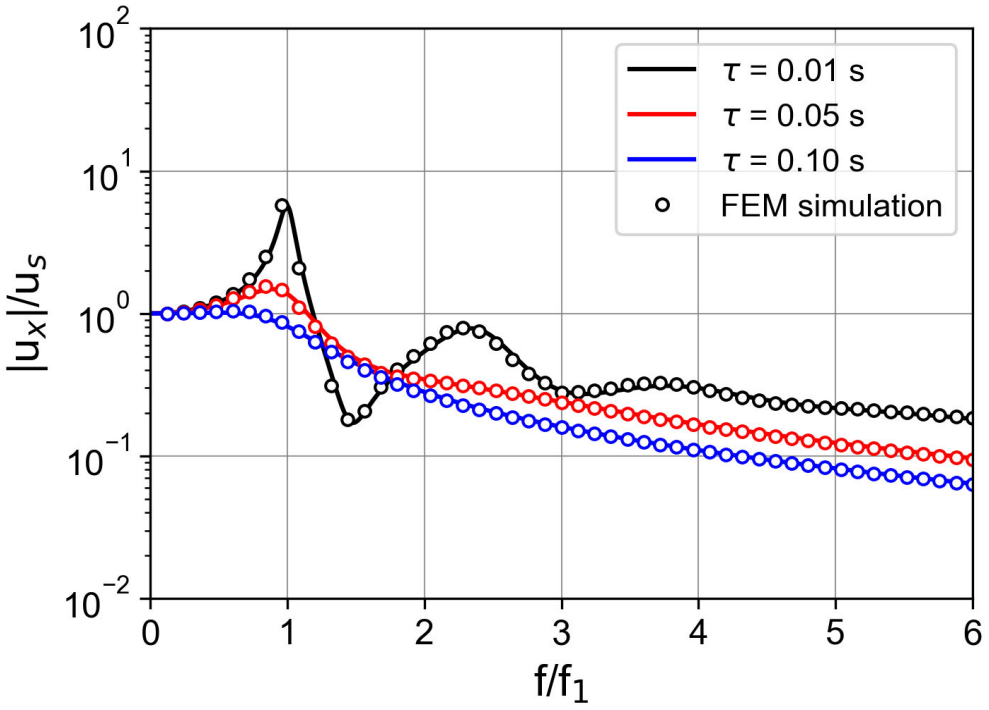

(a)

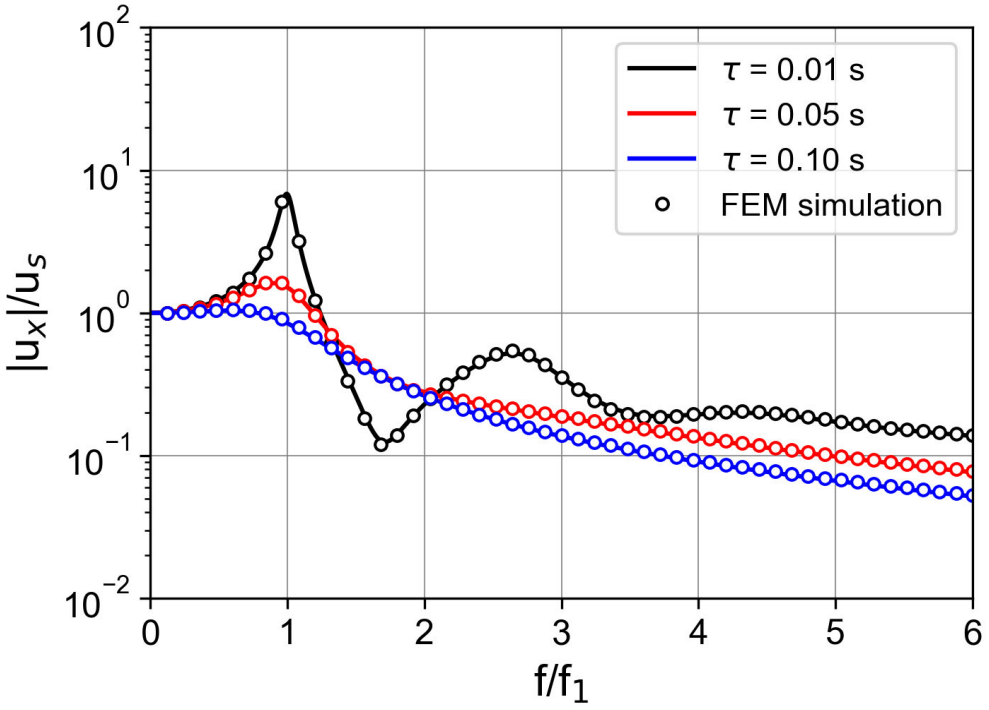

(b)

Figure 6. Comparison of the amplification factor at the ground surface between the present study and FEM simulation: (a) Type B with $z_0 = 10^0$ m, (b) Type C with $z_0 = 10^0$ m

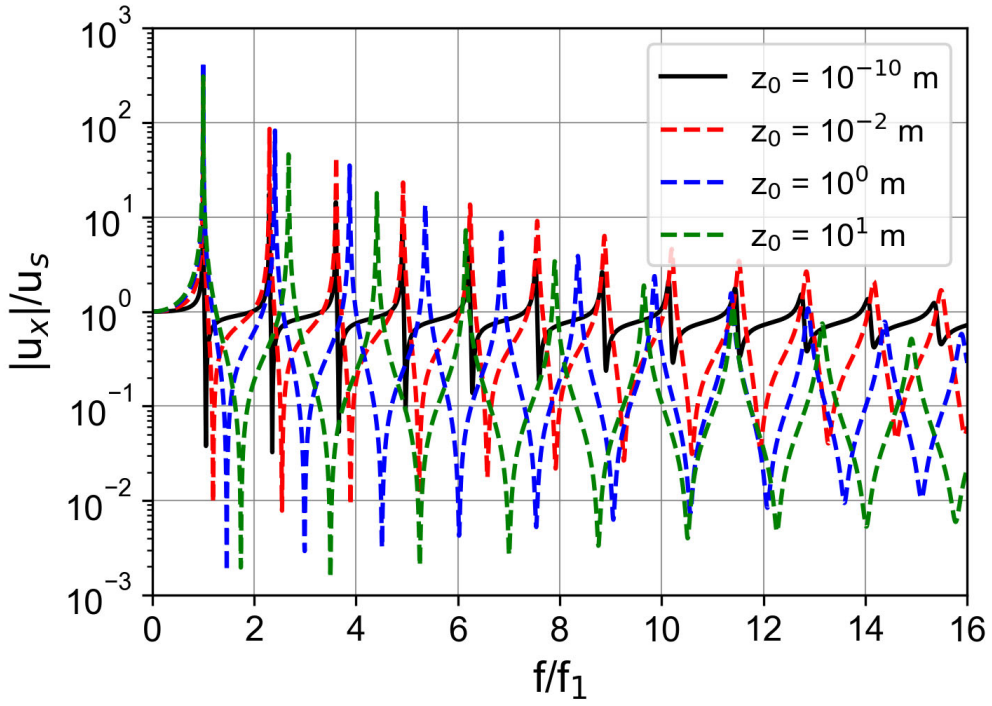
$z_0 = 10^{-10}$ m
$z_0 = 10^{-2}$ m
$z_0 = 10^{0}$ m
$z_0 = 10^{1}$ m
$|u_x|/u_s$
f/f_1

(a)

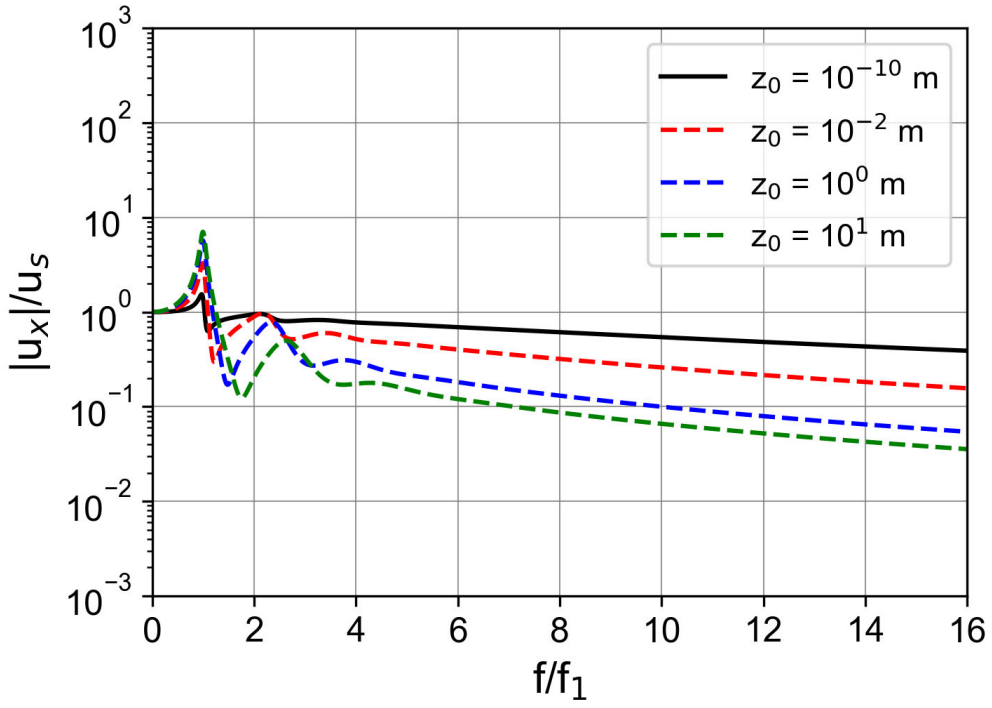
$z_0 = 10^{-10}$ m
$z_0 = 10^{-2}$ m
$z_0 = 10^{0}$ m
$z_0 = 10^{1}$ m
$|u_x|/u_s$
f/f_1

(b)

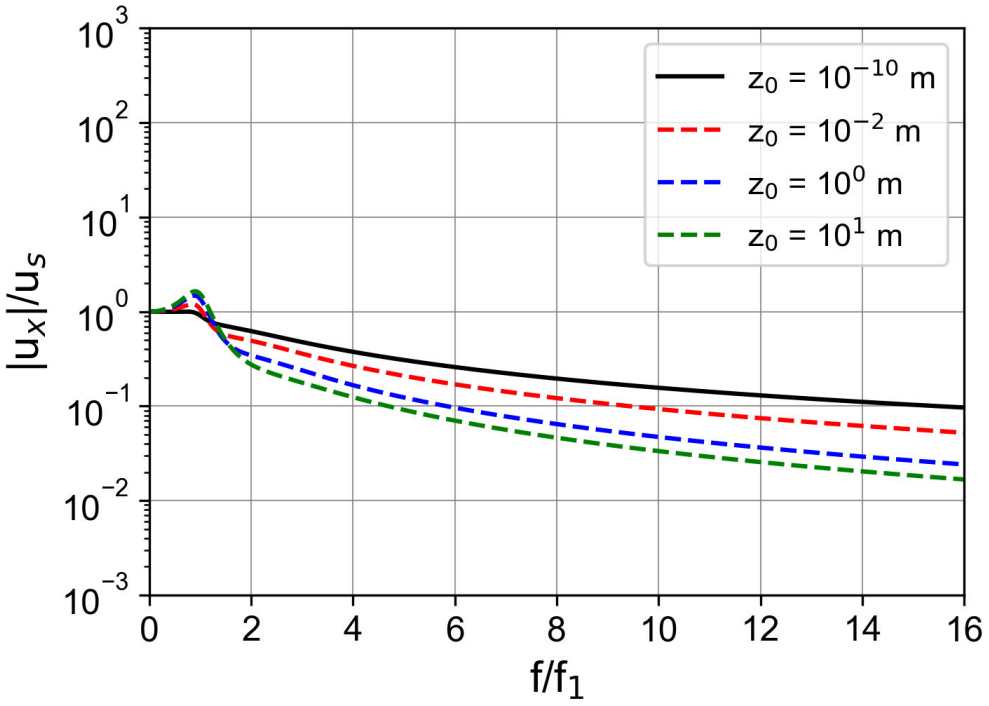

(c)

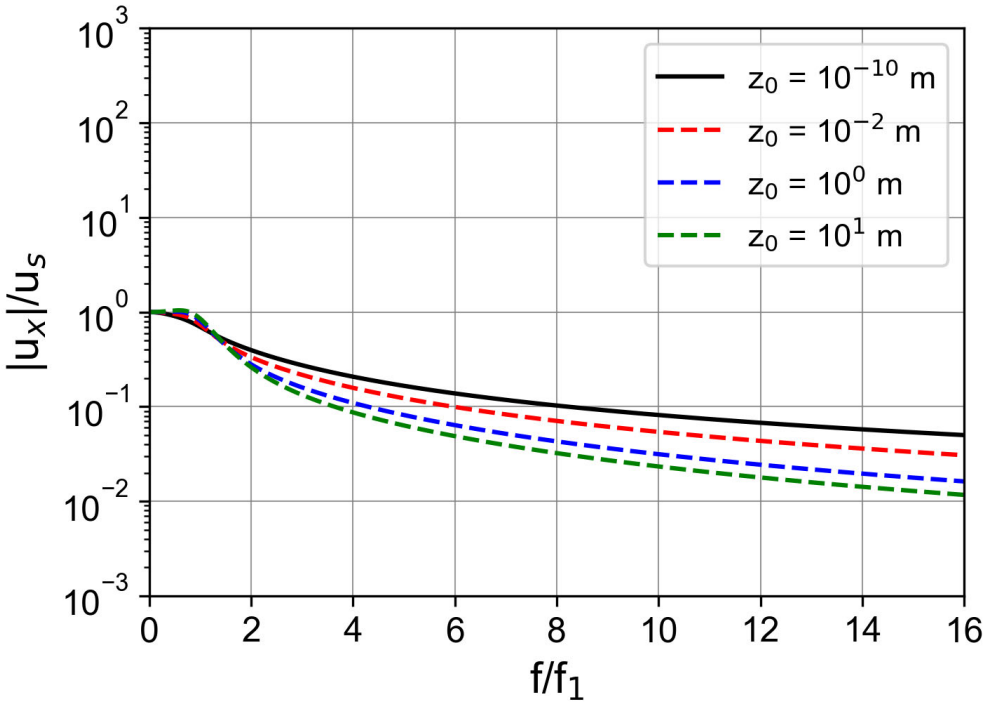

(d)

Figure 7. Effect of the parameter z_0 on the dynamic response at the ground surface under the horizontal stress loading at the ground surface for Type B with a different retardation time: (a) $\tau = 0.00$ s (poroelastic), (b) $\tau = 0.01$ s, (c) $\tau = 0.05$ s, (d) $\tau = 0.10$ s

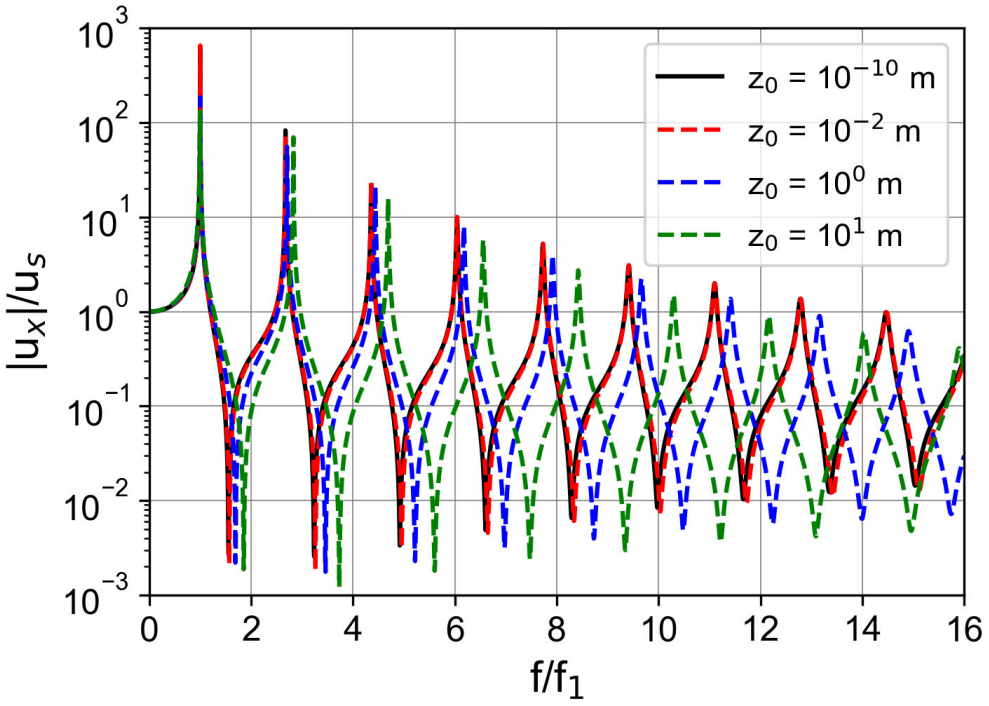
$z_0 = 10^{-10}$ m
$z_0 = 10^{-2}$ m
$z_0 = 10^{0}$ m
$z_0 = 10^{1}$ m
$|u_x|/u_s$
f/f_1

(a)

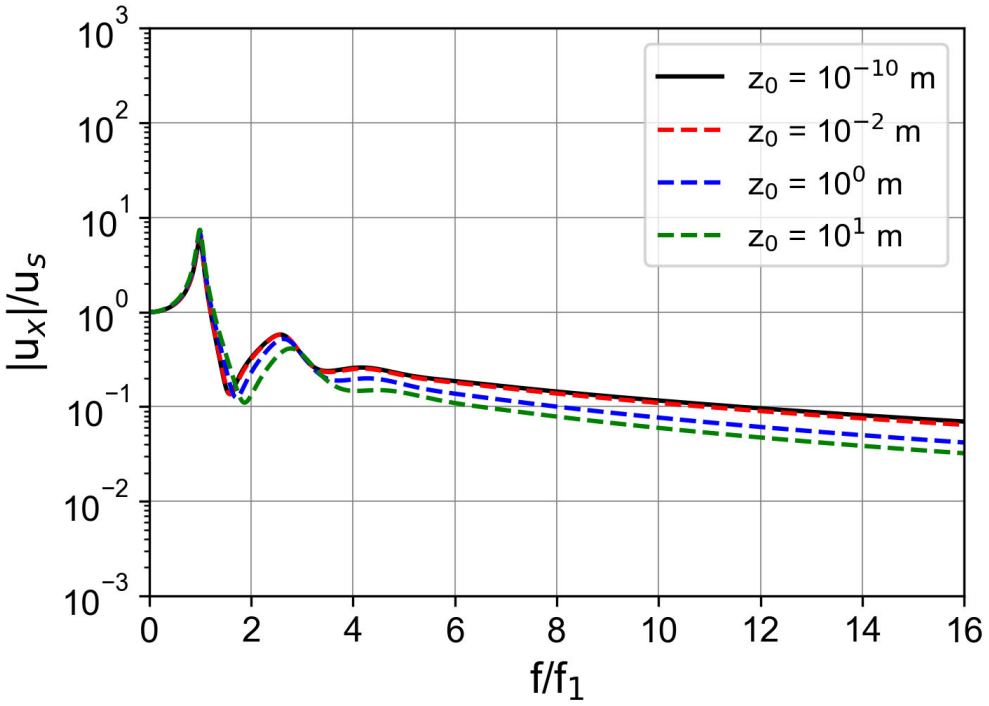
$z_0 = 10^{-10}$ m
$z_0 = 10^{-2}$ m
$z_0 = 10^{0}$ m
$z_0 = 10^{1}$ m
$|u_x|/u_s$
f/f_1

(b)

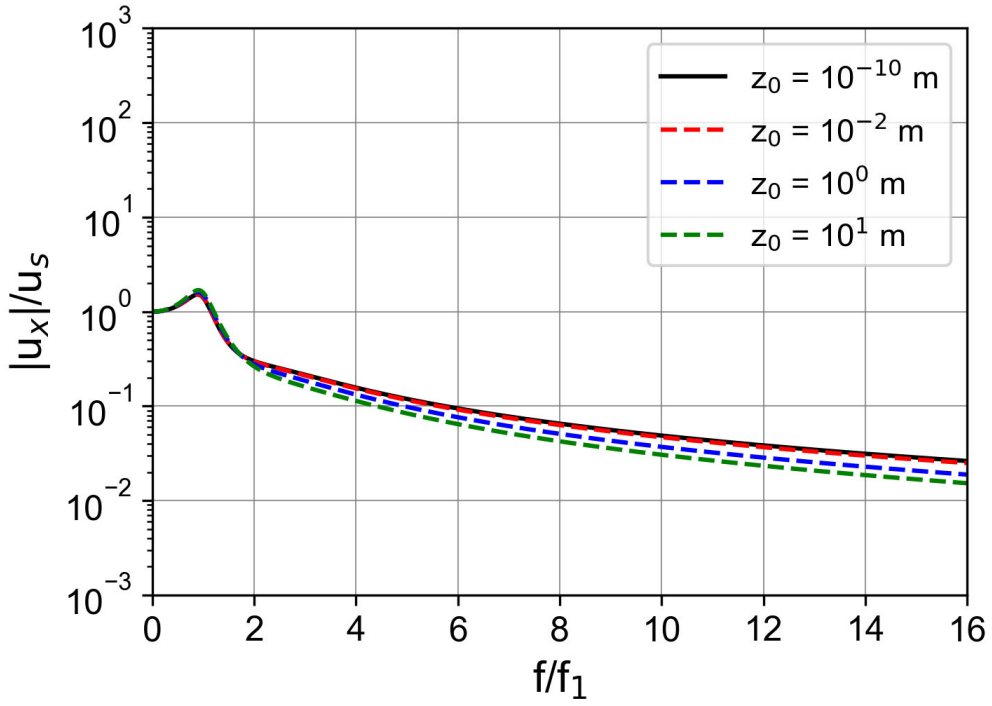

(c)

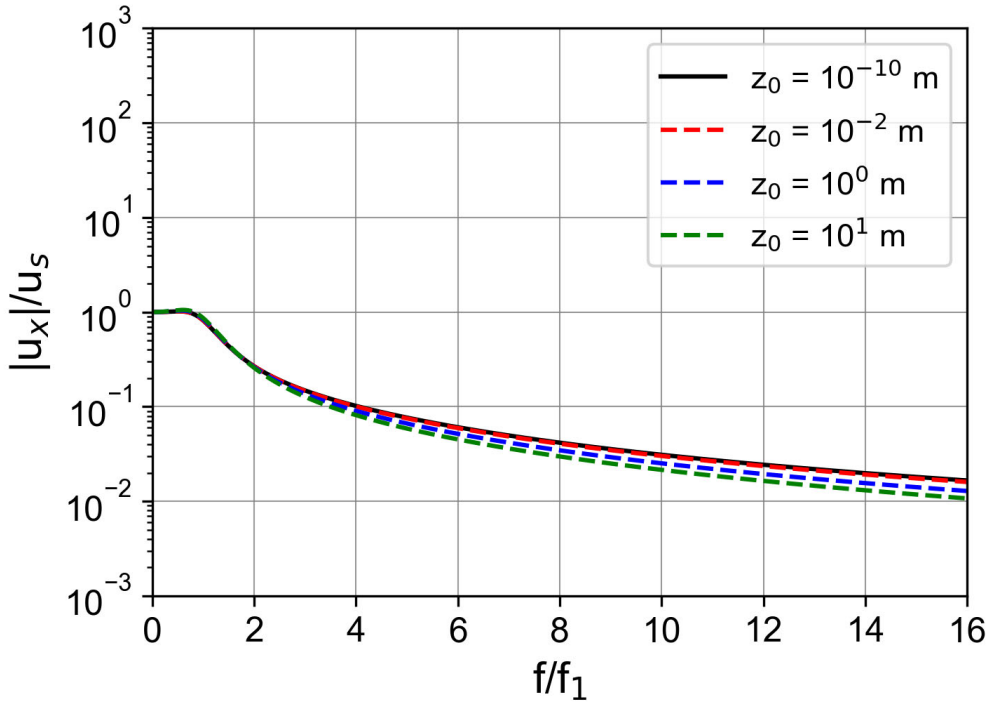

(d)

Figure 8. Effect of the parameter z_0 on the dynamic response at the ground surface under the horizontal stress loading at the ground surface for Type C ($m_G = 0.5$) with a different retardation time: (a) $\tau = 0.00$ s (poroelastic), (b) $\tau = 0.01$ s, (c) $\tau = 0.05$ s, (d) $\tau = 0.10$ s

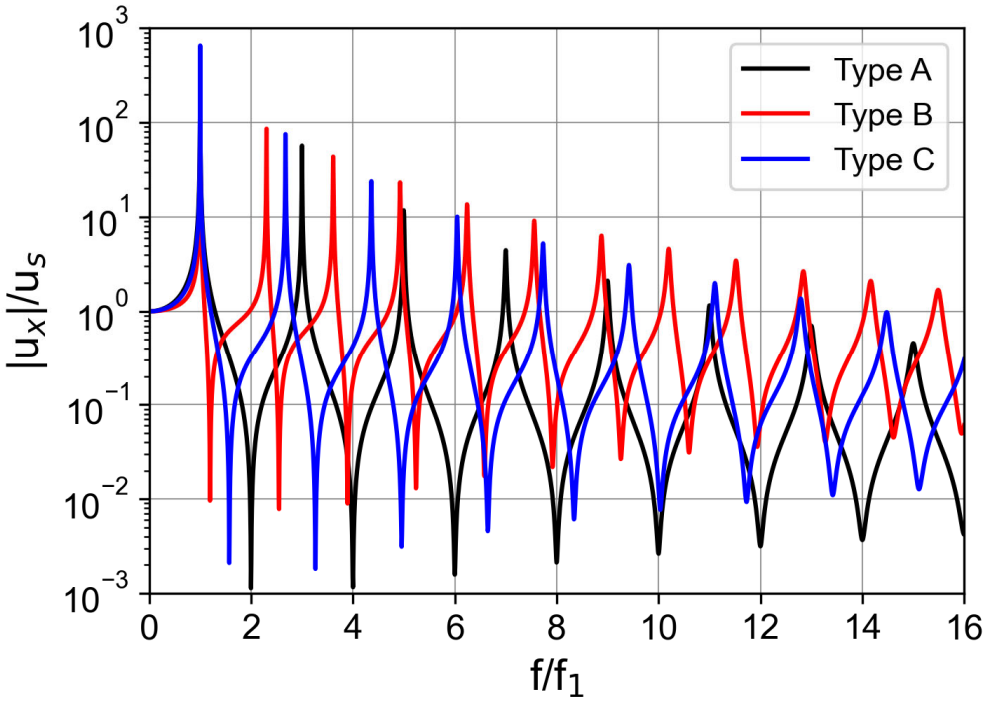

(a)

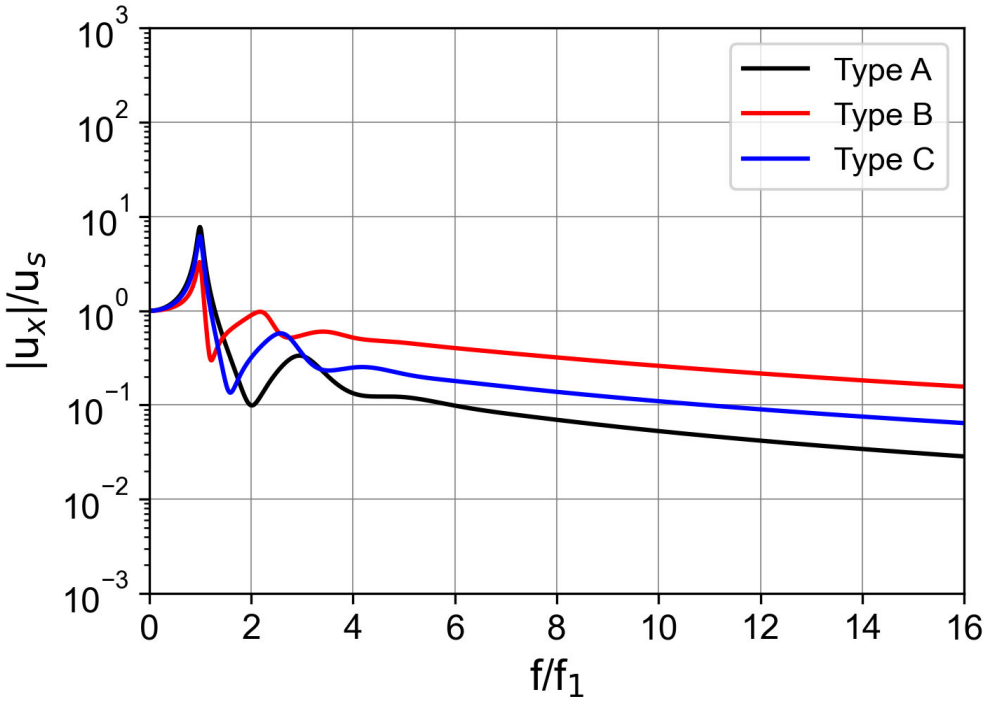

(b)

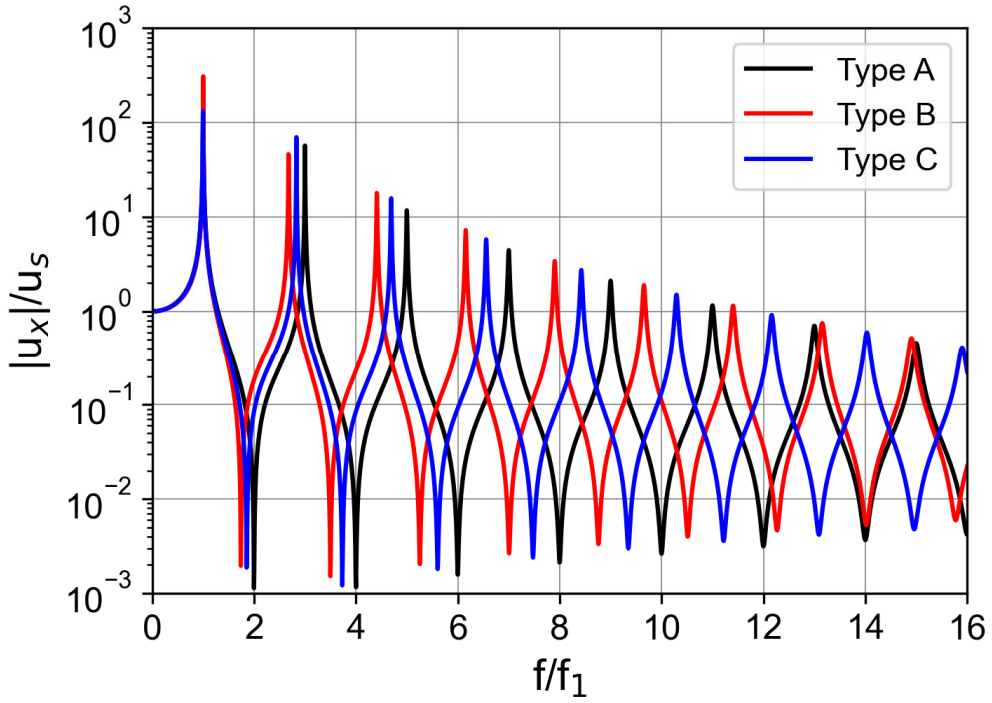

(c)

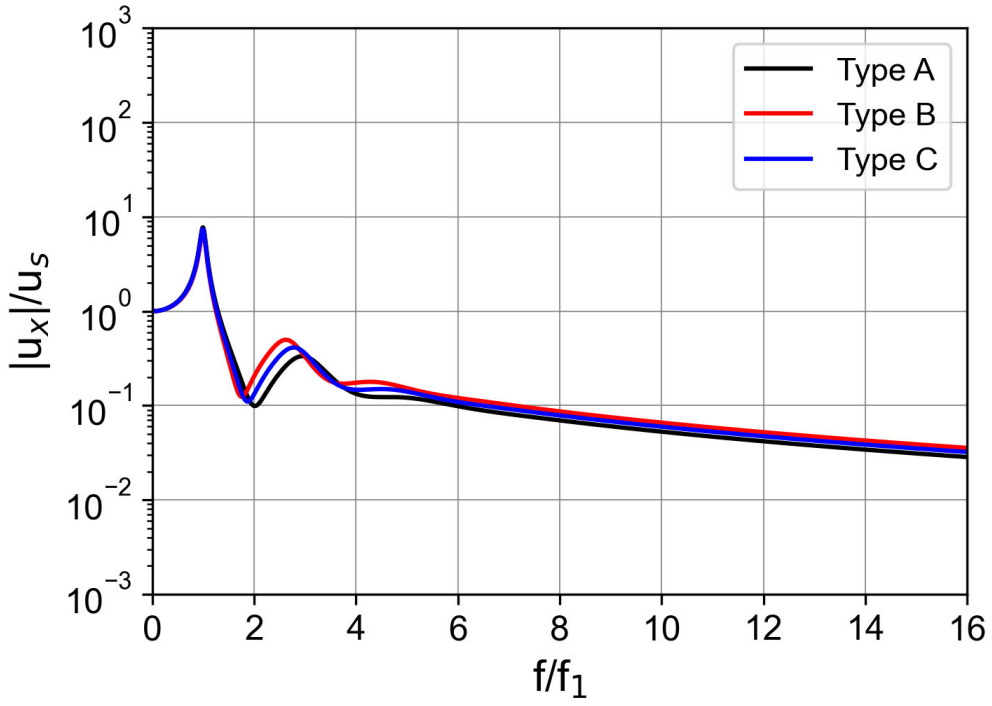

(d)

Figure 9. Effect of the Lame moduli's depth dependency on the dynamic response at the ground surface under the horizontal stress loading at the ground surface: (a) $\tau = 0.00$ s (poroelastic) with $z_0 = 10^{-2}$ m, (b) $\tau = 0.01$ s with $z_0 = 10^{-2}$ m, (c) $\tau = 0.00$ s (poroelastic) with $z_0 = 10^{1}$ m, (d) $\tau = 0.01$ s with $z_0 = 10^{1}$ m

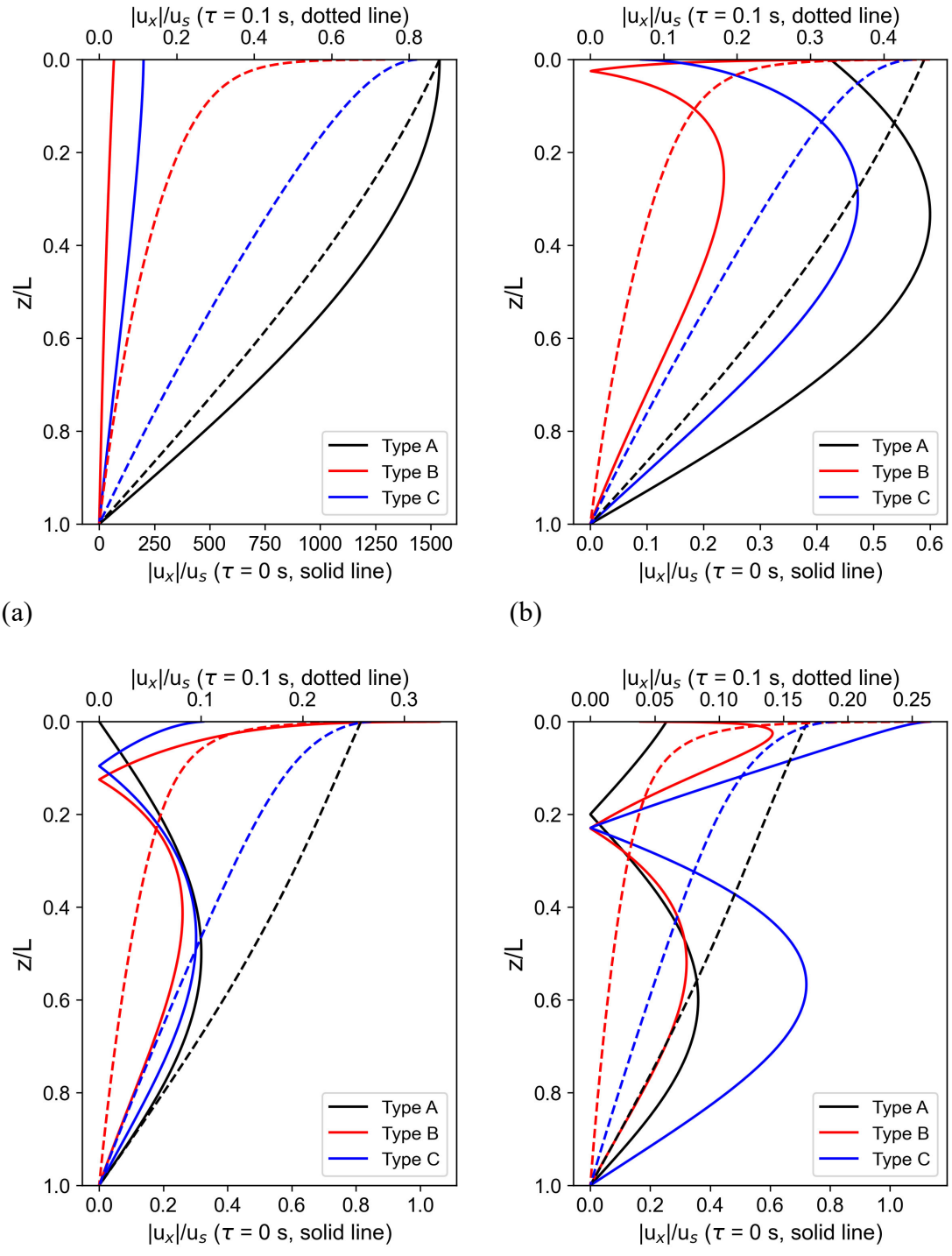

Figure 10. Effect of the Lame moduli's depth dependency and retardation time on the dynamic response depth profile under the horizontal stress loading at the ground surface ($z_0 = 10^{-2}$ m) at a different frequency: (a) $f/f_1 = 1.0$, (b) $f/f_1 = 1.5$, (c) $f/f_1 = 2.0$, (d) $f/f_1 = 2.5$, where f_1 is the first resonance frequency

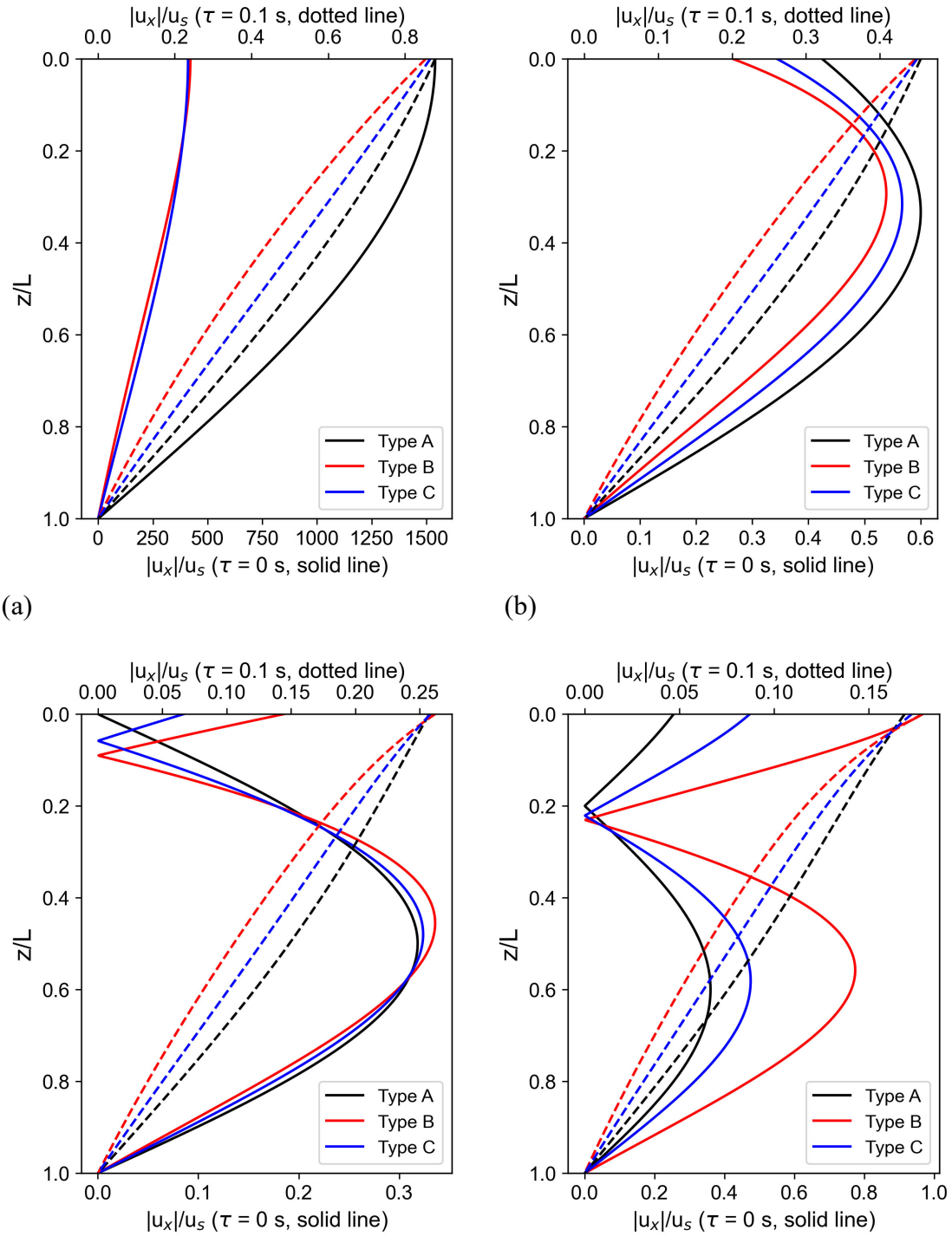

Figure 11. Effect of the Lame moduli's depth dependency and retardation time on the dynamic response depth profile under the horizontal stress loading at the ground surface ($z_0 = 10^1$ m) at a different frequency: (a) $f/f_1 = 1.0$, (b) $f/f_1 = 1.5$, (c) $f/f_1 = 2.0$, (d) $f/f_1 = 2.5$, where f_1 is the first resonance frequency

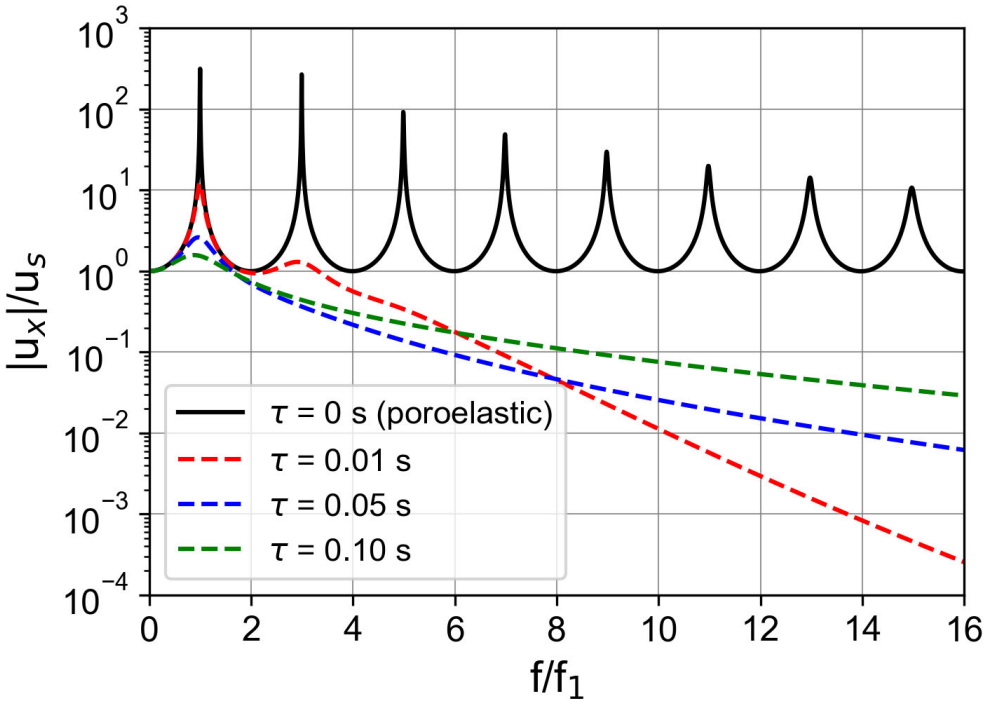

Figure 12. Effect of retardation time on the dynamic response at the ground surface under the horizontal bottom displacement loading for Type A

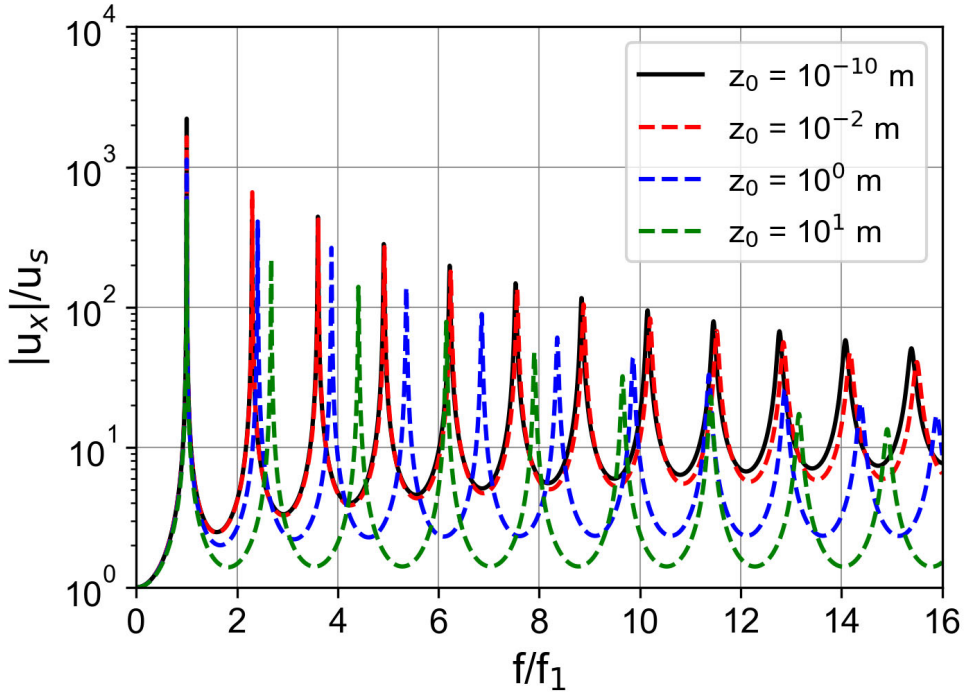
10^4
10^3
10^2
10^1
10^0
$|u_x|/u_s$
0
2
4
6
8
10
12
14
16
f/f_1
$z_0 = 10^{-10}$ m
$z_0 = 10^{-2}$ m
$z_0 = 10^0$ m
$z_0 = 10^1$ m

(a)

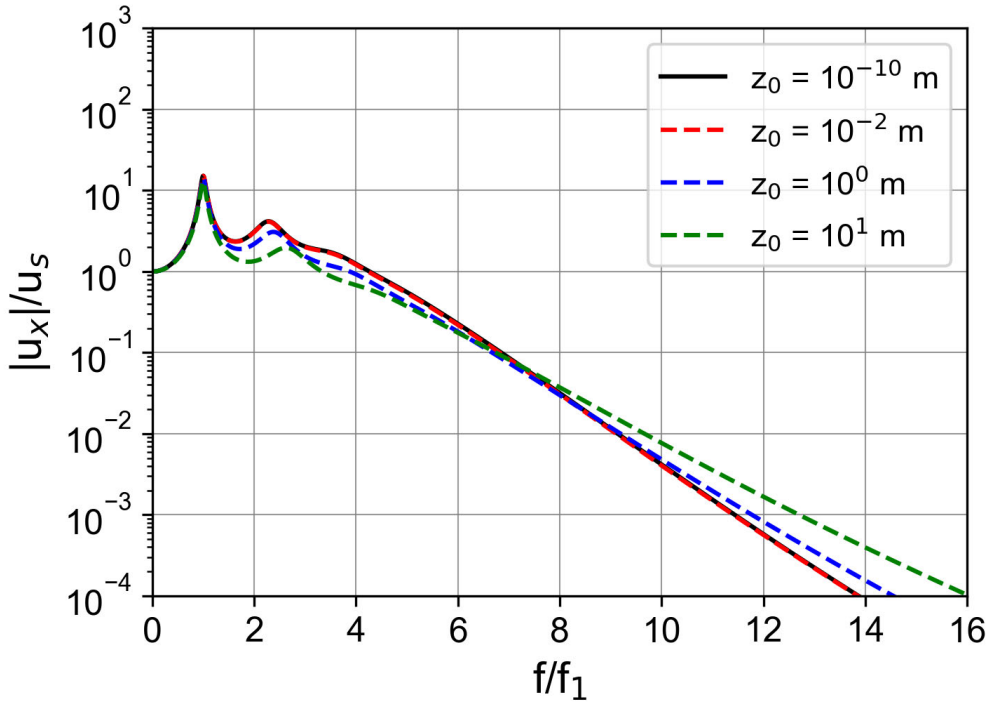
10^3
10^2
10^1
10^0
10^{-1}
10^{-2}
10^{-3}
10^{-4}
$|u_x|/u_s$
0
2
4
6
8
10
12
14
16
f/f_1
$z_0 = 10^{-10}$ m
$z_0 = 10^{-2}$ m
$z_0 = 10^0$ m
$z_0 = 10^1$ m

(b)

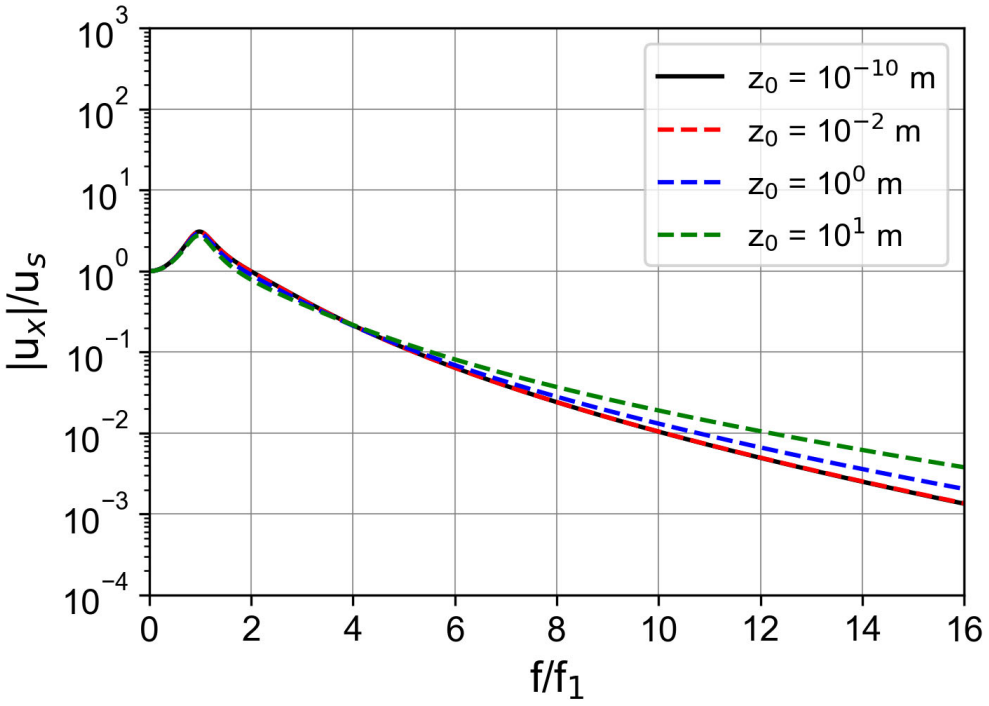

(c)

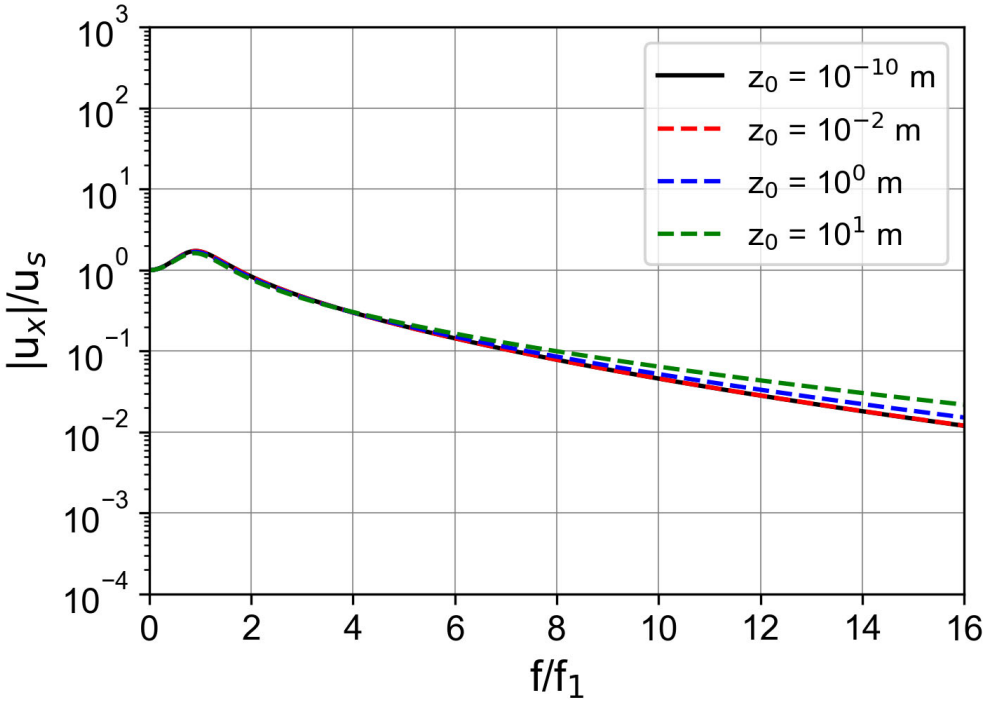

(d)

Figure 13. Effect of the parameter z_0 on the dynamic response at the ground surface under the horizontal bottom displacement loading for Type B with a different retardation time: (a) $\tau = 0.00$ s (poroelastic), (b) $\tau = 0.01$ s, (c) $\tau = 0.05$ s, (d) $\tau = 0.10$ s

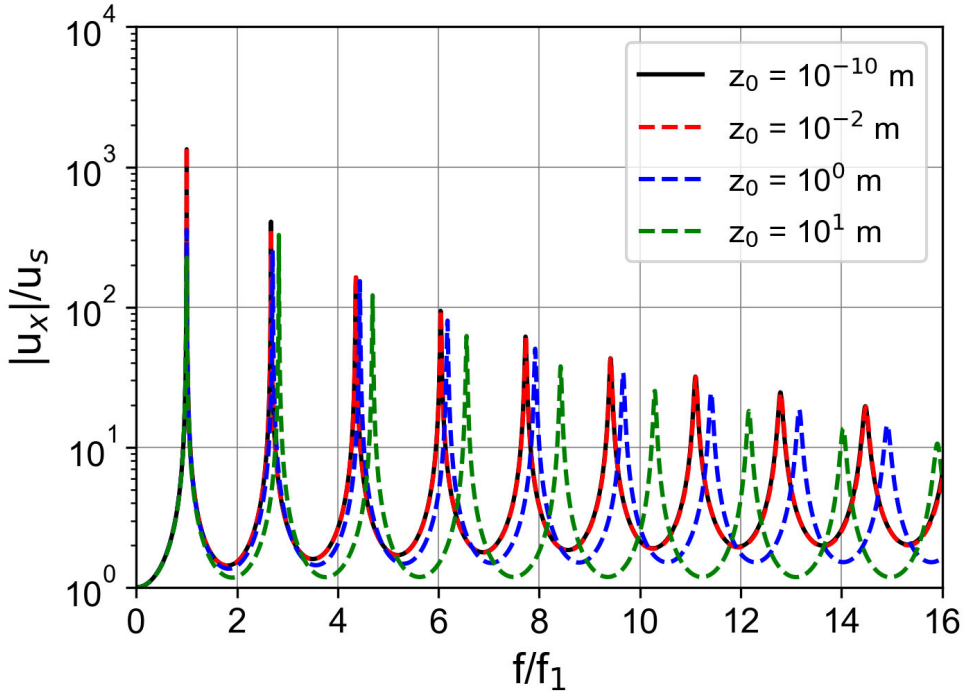
10^4
10^3
10^2
10^1
10^0
$|u_x|/u_s$
0
2
4
6
8
10
12
14
16
f/f_1
$z_0 = 10^{-10}$ m
$z_0 = 10^{-2}$ m
$z_0 = 10^0$ m
$z_0 = 10^1$ m

(a)

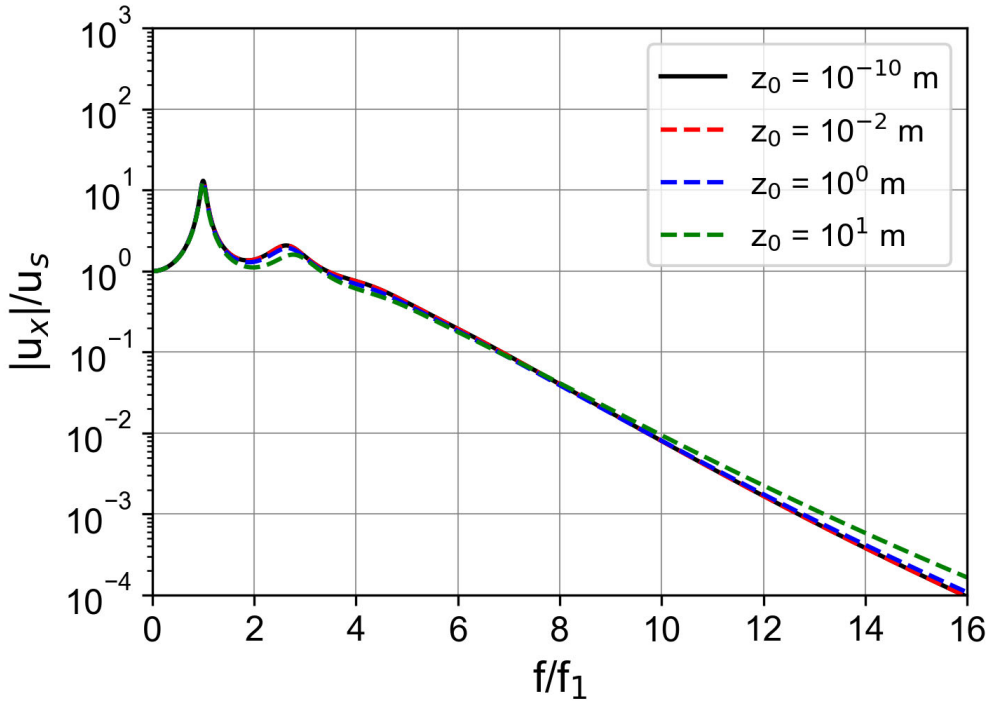
10^3
10^2
10^1
10^0
10^{-1}
10^{-2}
10^{-3}
10^{-4}
$|u_x|/u_s$
0
2
4
6
8
10
12
14
16
f/f_1
$z_0 = 10^{-10}$ m
$z_0 = 10^{-2}$ m
$z_0 = 10^0$ m
$z_0 = 10^1$ m

(b)

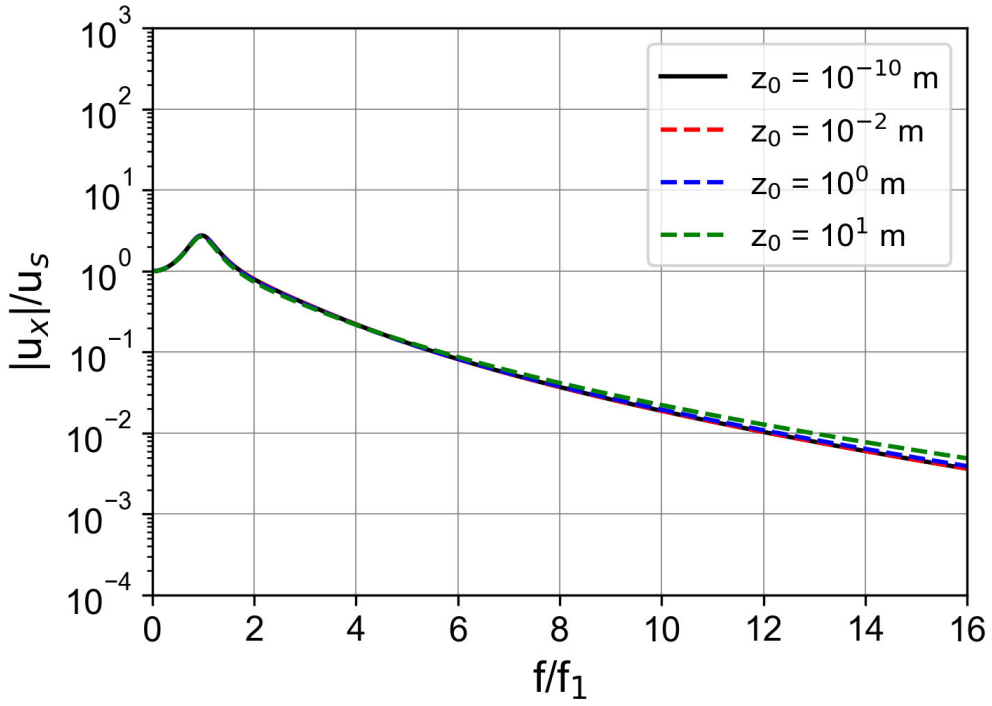

(c)

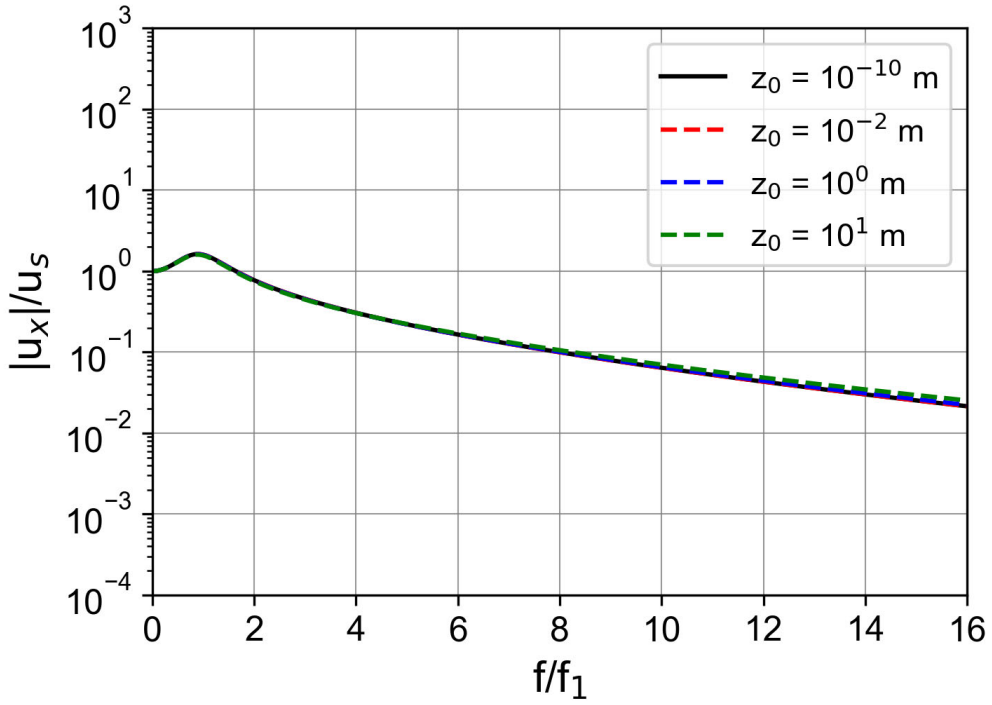

(d)

Figure 14. Effect of the parameter z_0 on the dynamic response at the ground surface under the horizontal bottom displacement loading for Type C with a different retardation time: (a) $\tau = 0.00$ s (poroelastic), (b) $\tau = 0.01$ s, (c) $\tau = 0.05$ s, (d) $\tau = 0.10$ s

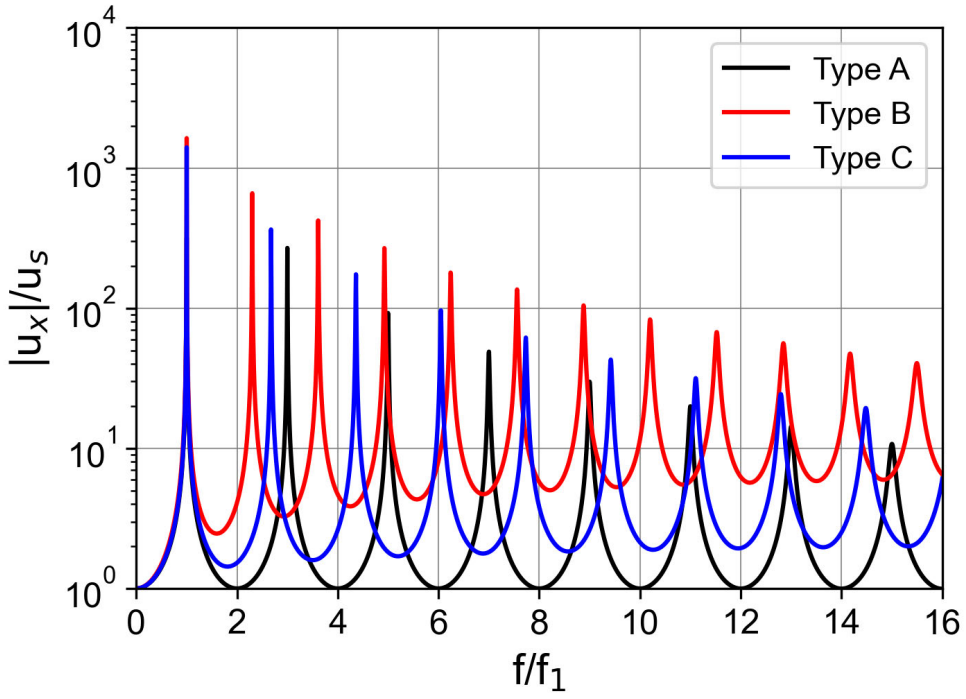

(a)

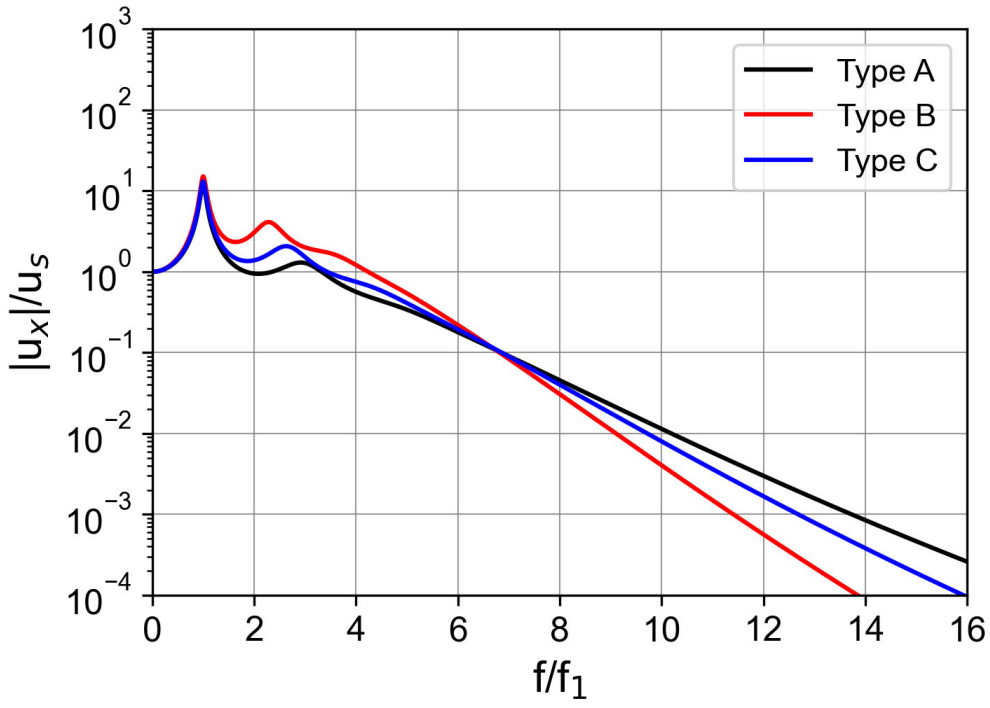

(b)

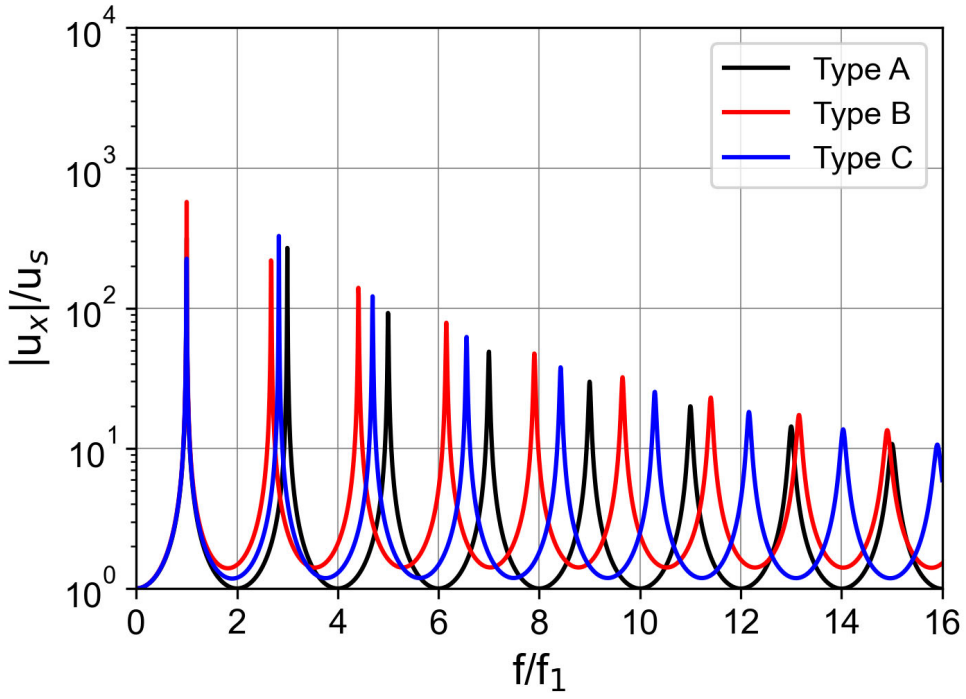

(c)

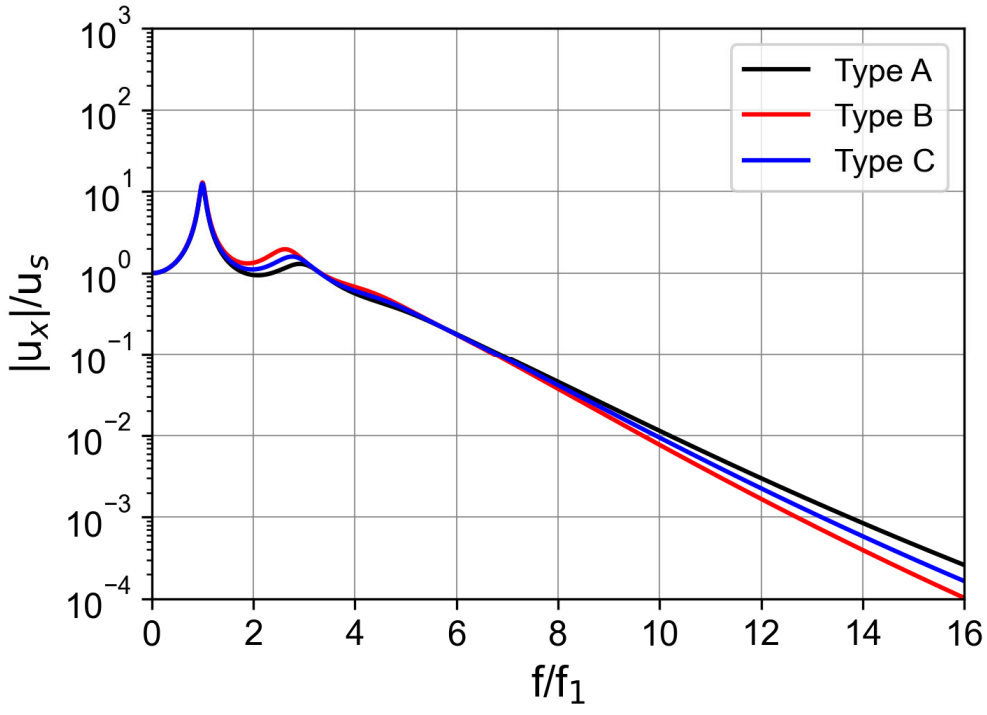

(d)

Figure 15. Effect of the Lame moduli's depth dependency on the dynamic response at the ground surface under the horizontal bottom displacement loading: (a) τ = 0.00 s (poroelastic) with $z_0 = 10^{-2}$ m, (b) $\tau = 0.01$ s with $z_0 = 10^{-2}$ m, (c) $\tau = 0.00$ s (poroelastic) with $z_0 = 10^{1}$ m, (d) $\tau = 0.01$ s with $z_0 = 10^{1}$ m

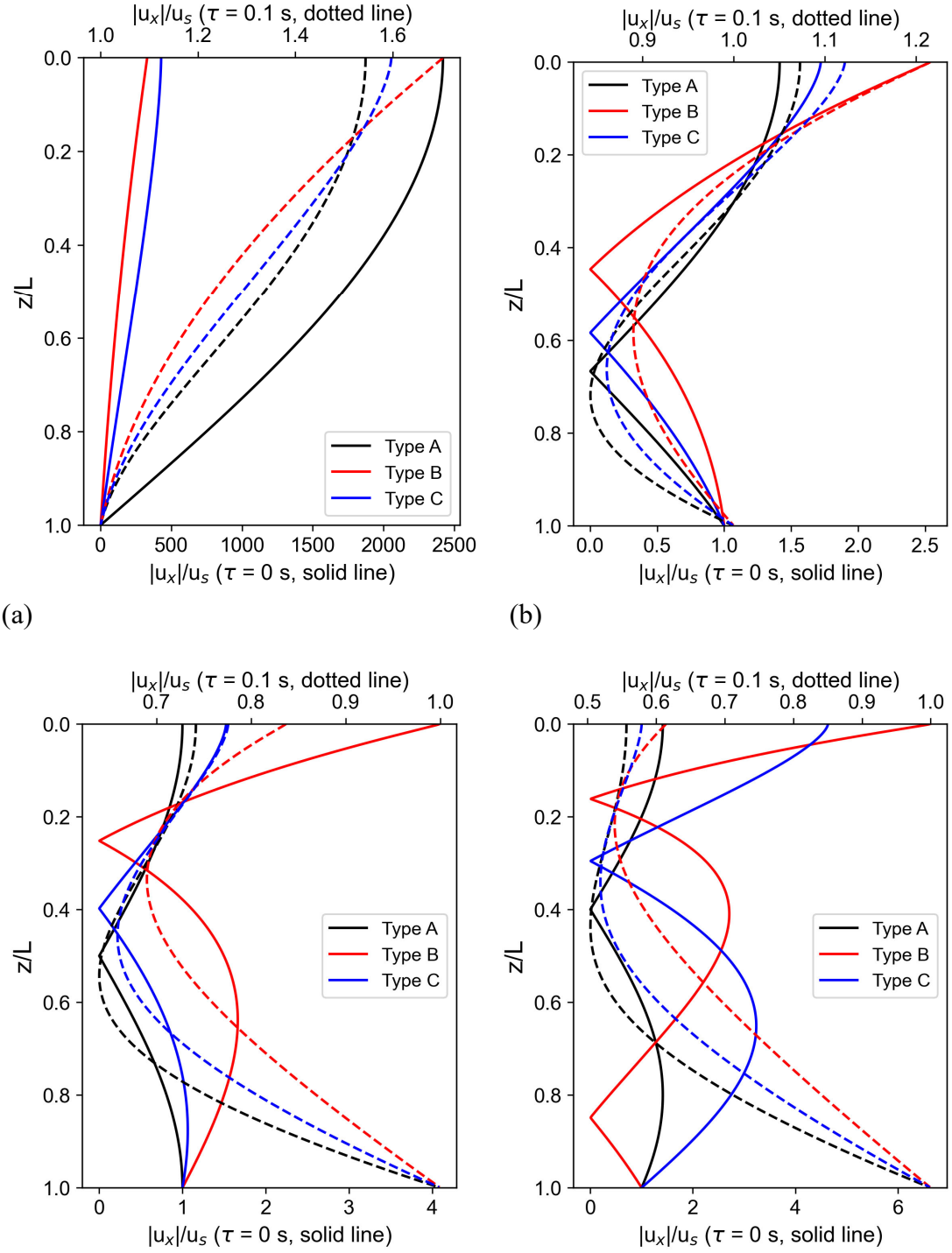

Figure 16. Effect of the Lame moduli's depth dependency and retardation time on the dynamic response depth profile under the horizontal bottom displacement loading (z_0 = 10^{-2} m) at a different frequency: (a) f/f_1 = 1.0, (b) f/f_1 = 1.5, (c) f/f_1 = 2.0, (d) f/f_1 = 2.5, where f_1 is the first resonance frequency

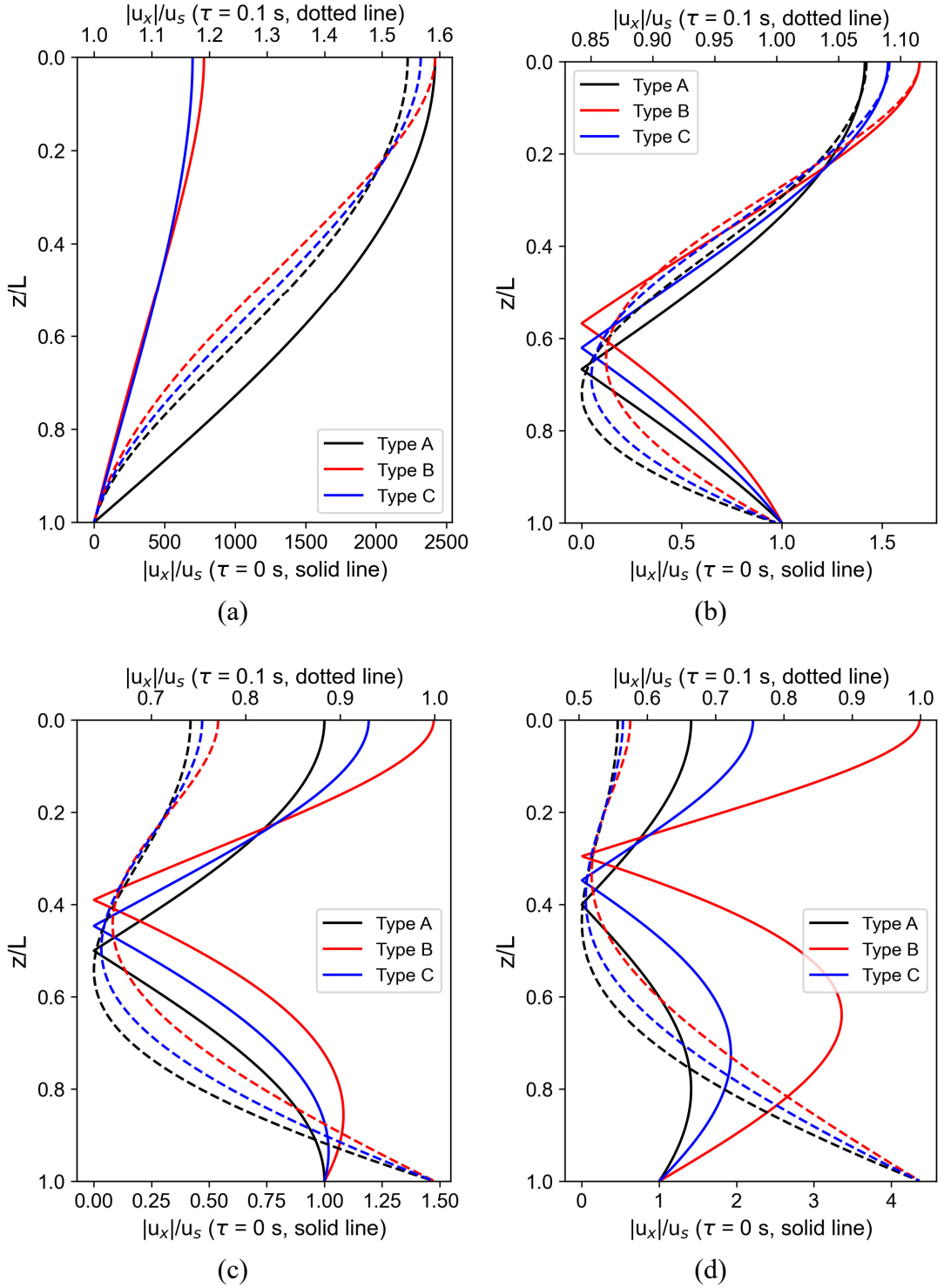

Figure 17. Effect of the Lame moduli's depth dependency and retardation time on the dynamic response depth profile under the horizontal bottom displacement loading (z_0 = 10^1 m) at a different frequency: (a) f/f_1 = 1.0, (b) f/f_1 = 1.5, (c) f/f_1 = 2.0, (d) f/f_1 = 2.5, where f_1 is the first resonance frequency